# AN ABSTRACT OF THE THESIS OF

Connor S. McCue for the degree of Master of Science in Materials Science presented on September 16, 2016.

Title: Development of Temperature-Stable Relaxor Dielectrics for High Energy Density Capacitor Applications

Abstract approved:

_____

David P. Cann

High performance dielectric materials are needed for high power SiC- or GaN-based electronics which combine the best features of high energy density, low dielectric loss and high reliability and for advanced high-speed and high-voltage energy storage where temperature stability plays an important role in material properties. An ideal capacitor for these systems features temperature-stable permittivity characteristics, a maximum permittivity near or below 0 °C, and sufficiently high permittivity to have practical application. This work involves the synthesis, processing, characterization, testing, and evaluating of the perovskite compositions $BaTiO_3$-$Bi(Zn_{1/2}Ti_{1/2})O_3$-$BiScO_3$-$NaNbO_3$, $BaTiO_3$-$Bi(Zn_{1/2}Ti_{1/2})O_3$-$Pb(Mg_{1/3}Nb_{2/3})O_3$, and $BaTiO_3$-$Bi(Zn_{1/2}Ti_{1/2})O_3$-$Pb(Ni_{1/3}Nb_{2/3})O_3$, all of which were investigated as possible linear dielectric capacitor materials. These materials have excellent dielectric properties due to a relaxor dielectric mechanism which is derived from B-site cation disorder. The characteristic diffuse phase transition observed in relaxor materials allows for a large temperature range of operation. These systems have been shown to have facile synthesis routes, creating single-phase solid solutions. The compositions studied have provided a framework for future work which would involve compositional modifications aimed at increasing the relative permittivity which would allow further device miniaturization as well characterization of the dielectric properties at high electric fields (E > 100 kV/cm).

# Development of Temperature-Stable Relaxor Dielectrics for High Energy Density Capacitor Applications

by
Connor S. McCue

A THESIS

submitted to

Oregon State University

in partial fulfillment of
the requirements for the
degree of

Master of Science

Presented September 16, 2016
Commencement June 2017

Master of Science thesis of Connor S. McCue presented on September 16, 2016

APPROVED:

Major Professor, representing Material Science

Head of the School of Mechanical, Industrial and Manufacturing Engineering

Dean of the Graduate School

I understand that my thesis will become part of the permanent collection of Oregon State University libraries. My signature below authorizes release of my thesis to any reader upon request.

Connor S. McCue, Author

# ACKNOWLEDGEMENTS

First and foremost, I would like to thank my major advisor, Dr. David P. Cann, for all the guidance and advice I have received throughout the course of my Master of Science. I couldn't have asked for a better boss. I would also like to thank my graduate committee for their patience in the completion of this thesis. I am privileged to have the opportunity to defend for you all.

Throughout the past two years, I have received a tremendous amount of assistance from graduate students, post-docs, and professors who have answered my questions, helped me solve problems, and pointed me in the right direction. Whether it was running to a stranger for equipment use or a general question asked at lunch, I was never turned away. I have enjoyed being a beaver and will miss the people I have met along the way.

Most importantly, I would like to thank my family for their constant love and support. I dedicate this thesis to them: Dad, my role model; Mom, my rock; and Molly, my pusher. I couldn't have done it without your love.

Funding for this work was provided by TRS Technologies, Inc.

# TABLE OF CONTENTS

Page

TABLE OF CONTENTS (Continued)

Page

# LIST OF FIGURES

# LIST OF TABLES

# Chapter 1 – Introduction

Ferroelectric relaxors are a type of dielectric material that exhibit interesting and useful electronic properties due to their highly diffuse phase transition. While all ferroelectrics go through a phase transition at their Curie temperature, most exhibit a sharp change in crystal structure. In contrast, relaxors exhibit a frequency dependent phase transition over a large range of temperature. Due to short range ordering of the B-site cations in the crystal structure, polar nano-regions are created that respond slowly to external stimuli, giving rise to their macroscopic material properties.

Relaxor ferroelectrics have many uses in modern technology; however, they are often limited to low temperature applications. New high performance dielectric materials are needed for more demanding applications that require materials which exhibit high energy densities, low dielectric losses, and high reliability over a wider temperature range. In order to develop ceramic capacitor materials with temperature-stable permittivity characteristics, lead-free $BaTiO_3$-$Bi(Zn_{1/2}Ti_{1/2})O_3$-$BiScO_3$-$NaNbO_3$ quaternary compositions and lead-based $BaTiO_3$-$Bi(Zn_{1/2}Ti_{1/2})O_3$-$Pb(Mg_{1/3}Nb_{2/3})O_3$ and $BaTiO_3$-$Bi(Zn_{1/2}Ti_{1/2})O_3$-$Pb(Ni_{1/3}Nb_{2/3})O_3$ ternary compositions were investigated to target a maximum permittivity and a temperature coefficient of relative permittivity approaching zero. These perovskite ceramic solid solutions were synthesized, evaluated, and modified to identify property trends so that their electronic properties can be optimized. The results achieved in this work demonstrate

that the electronic properties can be controlled based on composition and level of disorder. The optimum compositions exhibited a minimal temperature dependence and lower Curie temperatures, though the overall permittivity was decreased as a consequence.

Future work will involve additional compositional modifications aimed at increasing the relative permittivity which would enable device miniaturization as well characterization of the dielectric properties at higher electric fields (E > 100 kV/cm).

# Chapter 2 – Literature Review

A literature review with background information is included to provide relevant knowledge to this work. In this section, the history of capacitors and ferroelectrics will be discussed as well as relevant material characterization techniques.

## 2.1 Capacitors

A capacitor is a widely used electrical device that can temporarily store electric energy in an electric field. Commercial capacitors are typically manufactured using a solid dielectric material with high permittivity as a medium between two conductive materials. In the electronics world, they are called two-terminal elements due to having two places to connect to external circuits at each conductor. Capacitors are found in many different technologies for several reasons: they can store energy and are often used in power supplies; their operating voltage is proportional to the charge stored so a capacitor can be used to perform complicated computations in operational amplifier circuits; and circuits built with capacitors exhibit frequency-dependent behavior allowing for tunable amplification. In modern society, capacitors often go unnoticed but are found in nearly every consumer electronic and circuit board.

In October of 1745, a German scientist named Ewald George von Kleist discovered that an electric charge could be stored by connecting a high-voltage electrostatic generator to a jar of water by wire (Keithly, 1999). The following year, a Dutch scientist out of Leyden by the name of Pieter van Musschenbroek used the

principles found by Kleist to create a similar device that stored an electric charge in a jar of water, called a Leyden jar (Keithly, 1999). It was the first example of electrical energy storage of static energy and has all the elements of a modern capacitor: two conducting plates separated by an insulator. The first practical use of capacitors arose with the invention of the wireless radio in the late 19$^{th}$ century, and they have had a place in technology ever since.

## 2.2 Capacitance

Capacitance is defined as: the ability of a system to store an electric charge. The SI unit for capacitance is the Farad (F) named after English physicist Michael Faraday and is equal to the capacitance of a capacitor when one volt of potential difference stores one coulomb of charge. Unfortunately, the Farad is an unreasonably large standard unit, so it is more commonly measured in picoFarads or nanoFarads. The Farad is defined as:

$$C = \frac{q}{V}$$

where q is the internal charge stored and V is the voltage across the capacitor. The most common form of capacitor is a parallel plate capacitor, where two conductive plates are placed on the outside of an insulating material. To find the capacitance, an AC voltage is applied to the sample at the electrodes and the stored charge is

measured. For this geometry, the capacitance of the sample is defined by the equation:

$$C = \frac{\varepsilon_0 \varepsilon A}{t}$$

where $\varepsilon_0$ is the permittivity of free space (8.8514 x $10^{-12}$ F/m), ε is the relative permittivity (unitless) of the dielectric material across the sample, t is the thickness of the ceramic pellet (m), and C is the capacitance of the sample (F). A material's permittivity is measured relative to vacuum. The relative dielectric permittivity (κ) is thus the ratio relative of the permittivity of the dielectric to the permittivity of free space and is defined as:

$$\kappa = \frac{\varepsilon_{ij}}{\varepsilon_0}$$

The dielectric permittivity has two parts: real and imaginary. The imaginary permittivity corresponds to the dielectric loss (and is often associated with heat). The dielectric loss of a material is related to its ability to dissipate electromagnetic energy in the form of heat. It also plays an important role is the measurement of the dielectric properties. Typically, the dielectric loss is reported in terms of the loss angle or loss tangent (tan δ) and it is usually a strong function of frequency. The imaginary part accounts for the loss in the material due to damping of vibrating dipole moments dispersed through the system as heat, lossless dielectrics have a zero imaginary permittivity.

## 2.3 The Development and History of Advanced Piezoelectric Materials

The direct piezoelectric effect, the ability of a material to generate an electric charge in response to an applied stress, was first discovered in 1880 by brothers Jacques and Pierre Curie (Kolkin & Goltsev, 2008). They had discovered an unusual phenomenon in several crystals, including cane sugar, topaz, and quartz. When subject to a mechanical force, these crystals became electrically polarized. The voltage was proportional to the applied force, and compression and tension created potentials of opposite polarity. The converse effect, when an applied voltage created a mechanical response, was also confirmed true and named the converse piezoelectric effect. The term piezoelectric comes from the Greek word *piezein*, meaning to press or squeeze.

The first material to be utilized for its piezoelectricity is quartz. During World War I, Germany was reliant on imports for food and fertilizer to feed its citizens (Koerver, 2012). The United Kingdom, with its superior navy, blockaded Germany to prevent necessary supplies from reaching continental Europe. The German Navy turned towards U-boats, i.e. submarines, to break the blockade and attack British supply lines. Over the course of the war, the Allies suffered heavy losses as U-boats patrolled the North Atlantic, creating absolute havoc and losing thousands of tons of supplies and lives (Koerver, 2012). The situation looked bleak – there was no consistent way to find a submerged U-boat. In 1917, a French physicist named Paul Langevin, a student of Pierre Curie's, developed the first practical application of the piezoelectric effect by sending high-frequency electric signals through a quartz

crystal, which produced a mechanical stress (Zimmerman, 2002). He created what would be today called a transducer, a device that converts electrical signals to an acoustic wave or vice versa. A quartz crystal was used to create high frequency sound waves, and a microphone was used to hear the echoes. By calculating the time difference, one could calculate the distance the sound waves traveled. While not necessary to winning the war, sonar is still a mainstay in modern submarines.

Piezoelectricity is defined by the piezoelectric coefficient ($d_{ij}$) which quantities the volume change of a material which is subject to an electric field or vice versa. This is represented mathematically as:

$$d_{ij} = \frac{induced\ polarization}{applied\ mechanical\ stress}$$

The larger the change in mechanical displacement and therefore the displacement of dipoles (i.e. polarization), the higher a material's piezoelectric coefficient. Since strain is a second rank tensor and the applied electric field is a first rank tensor, the piezoelectric coefficient $d_{ij}$ is a third rank tensor, and so there are numerous piezoelectric coefficients to a material. The most widely used coefficient to describe a material's response to external stimuli is the $d_{33}$ coefficient, which describes the induced strain in the direction parallel to polarization per unit of applied electric field.

Quartz is the second most abundant mineral on Earth, so it's not surprising that it was one of the first materials where the piezoelectric effect was observed. However, its piezoelectric coefficient is relatively low, $d_{33}$ = 2.33 pC/N. Quartz

remained the material of choice for many applications, including filters for radio transmitters and receivers, resonators, and time keeping. In the 1960s, research into single crystal piezoelectric resurged with the discovery of lithium niobate ($LiNbO_3$) (i.e. LN) and lithium tantalate ($LiTaO_3$) (i.e. LT), eventually replacing quartz due to their superior piezoelectric properties, an electromechanical coupling factor five times higher than quartz, and great toughness and hardness (Smith R. T., 1967) (Yamada, Niizeki, & Toyoda, 1967). The similar electronic properties of LN and LT are not surprising because niobium and tantalum are almost chemically identical.

## 2.4 Perovskites

The perovskite structure is a highly versatile and useful crystal structure that is widely studied in solid-state inorganic chemistry. Understanding the importance of the perovskite crystal structure will explain why ferroelectricity is so common in these materials. Perovskites were first discovered in 1839 by Gustav Rose, a German mineralogist working in the Ural Mountains in Russia: he first found calcium titanate ($CaTiO_3$) and coined the term perovskite after Lev Perovski, a Russian mineralogist (Chakhmouradian & Woodward, 2014). The classic perovskite chemical formula is $ABX_3$, where A is a 12-fold coordinated metal cation, B is a 6-fold coordinated metal cation, and X is an anion, usually oxygen (Smith, et al., 2008). The crystal structure of perovskites was discovered using X-Ray diffraction by Helen Dick Megaw in 1945 on barium titanate (Chakhmouradian & Woodward, 2014).

The Goldschmidt tolerance factor is a measure of the packing of the A-site cations into the geometrically octahedral framework provided by the B-site cations. For an ideal cubic structure, the tolerance factor is one and the lattice parameter is equal to two times the B – X bond length and the A – X bond is the cross sectional diagonal of the cube. The tolerance factor (t) is defined as:

$$t = \frac{R_A + R_X}{\sqrt{2}(R_B + R_X)}$$

where; t = tolerance factor, $R_A$ is the ionic radii of the A-site cation in 12-fold coordination, $R_B$ is the ionic radii of the B-site cation in 6-fold coordination, and $R_x$ is the ionic radii of the anion. In this arrangement, the tolerance factor describes the physical arrangement of the structural cations and anions in 3-dimenional space. When t = 1, the unit cell exhibits a cubic structure and all ions are of ideal size for perfect packing (e.g. $SrTiO_3$). For all other tolerance factors, the perovskite structure is distorted; the $BO_6$ octahedral tilts or distorts and the A-site cation is displaced. When t > 1, the unit cell is distorted due to the large size of $R_A$ in relation to $R_B$. A cubic structure is not possible, and perovskites of this nature are typically hexagonal or tetragonal (e.g. $BaNiO_3$, $LaAlO_3$). When t < 1, the unit cell is distorted due to small size of $R_A$ in relation to $R_B$. Perovskites of this nature are typically exhibit rhombohedral or orthorhombic symmetry (e.g. $CaTiO_3$).

Distorted perovskites have reduced symmetry, allowing for interesting electric and magnetic properties. Ferroelectricity is a product of anisotropy and can only

happen in materials if the following conditions must occur: the unit cell must be non-centrosymmetric and polar. All ferroelectric ceramics are drawn from materials which meet both of those requirements.

The ideal cubic perovskites structure can be visualized with $SrTiO_3$. In a classic cubic $ABX_3$ perovskite system, the space group is Pm-3m, the Wyckoff positions are: the A cation is at ( ½, ½, ½ ); the B cation is at ( 0, 0, 0 ), and the X atoms are in 3d ( ½, 0 , 0 ), ( 0, ½, 0), ( 0, 0, ½ ). However, the perovskite structure is very flexible and can accommodate a large variety of cation sizes. As such, most perovskites are not cubic and exhibit some level of distortion. Often this allows for easily identifiable phase changes due to a change in temperature. For ferroelectrics, this is often characterized by a tetragonal to cubic phase transition which happens at a specific temperature called the Curie temperature ($T_C$). The magnitude of $T_C$ depends on the chemistry of the A-site and B-site and their electronic structure.

For example: $BaTiO_3$ has four different structural distortions: it is stable in the rhombohedral structure below -90°C, it is orthorhombic between -90°C and 5°C, tetragonal between 5°C to 120°C, and it is stable in the cubic structure at temperatures above 120°C. In the $BaTiO_3$ system, the ferroelectric to paraelectric phase transition occurs at 120°C with the tetragonal phase being host to the ferroelectric phase and the cubic phase is the parent paraelectric phase.

## 2.5 Ferroelectricity and Barium Titanate (BT)

Ferroelectricity is the material property where a material becomes spontaneously polarized in the absence of an electric field. This dipole moment can be re-oriented upon application and an electric field, and is retained once the electric field is removed. Typical ferroelectric materials go through a phase transition at a specific temperature, called the Curie temperature, where they transition from a ferroelectric phase to a paraelectric phase, and often from tetragonal symmetry to cubic symmetry respectively. A ferroelectric crystal has two crystal symmetry requirements: it cannot be centrosymmetric and must have a unique polar axis. The spontaneous polarization disappears as the unit cell transforms into cubic symmetry, with a centrosymmetric character. Out of the 32 crystalline classes, 20 are non-centrosymmetric and piezoelectric, and only 10 of those are pyroelectric (polar).

The discovery of ferroelectricity in mixed oxide perovskites was a large turning point in the history of electronic ceramics. Previously, ferroelectricity had only been identified in two crystals, Rochelle salt and potassium dihydrogen phosphate, both chemically unstable. During World War II, Arthur Von Hippel discovered ferroelectricity in barium titanate ($BaTiO_3$) ceramics (Zahn, 1988). This opened the door for other mixed oxide perovskites to be studied, with ferroelectricity being found in many including – importantly – lead titanate ($PbTiO_3$).

Prior to the discovery of ferroelectricity in ceramic barium titanate, ceramic materials were rarely used in capacitor technology. Current capacitors are fabricated

with multiple dielectric layers electrically connected in parallel, with thicknesses around 1.5 µm, to increase capacitance. Typically, nickel internal electrodes are used to reduce cost and to enhance the mechanical integrity of the devices. An example of a typical multi-layer capacitor setup is shown below:

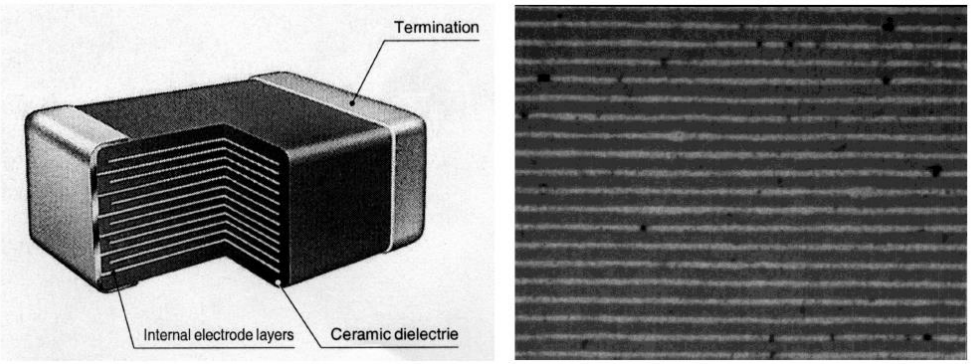


Figure 2.1 - Normal structure for a multilayer capacitor (left) and micron-scaled layers made from doped barium titanate and nickel electrode layers (Randall, 2004)

The growth of $BaTiO_3$ crystals were first produced in 1947, but it took seven years to obtain crystals grown well enough to study. In 1954, Remeika produced large crystals of $BaTiO_3$ that allowed the scientific community to study the material's fundamental properties, including: dielectric anisotropy, domain switching, and the electro-optical and electromechanical properties (Remeika, 1954). This new step in studying ferroelectrics allowed for easier measurements and scientific work on $BaTiO_3$, which is an ideal ferroelectric perovskite. In 1949, for the first time, Merz *et al.* carried out polarization and permittivity measurements on $BaTiO_3$ crystals in order to characterize the fundamental properties of this material (Merz W. , 1949). Below

shows one of the first optical micrograph pictures of 90° domain walls in single crystal barium titanate (Forsbergh, 1949).

To better understand the $BaO$-$TiO_2$ phase equilibria, its phase diagram was first investigated by Rase and Roy (Rase & Roy, 1955). They found five intermediate $BaO$-$TiO_2$ compounds that existed in the system. Near the compound $BaTiO_3$, excess titania ($TiO_2$) will not appear as a secondary phase but will rather incorporate itself into the pre-existing perovskite structure, allowing for a higher solubility of titania in this composition (up to 2 to 3% mole excess). An updated phase diagram of barium titanate is shown below (Lee, Randall, & Liu, 2009):

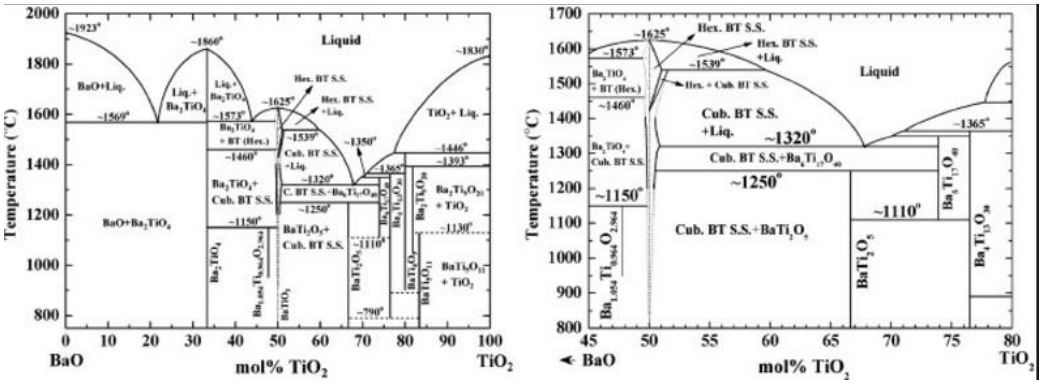


Figure 2.2 - Complex phase diagram of $BaO$-$TiO_2$ **(Rase & Roy, 1955)**

Ceramics based on $BaTiO_3$ have been used in a wide variety of applications in various forms; crystals, bulk ceramics, multilayers, and thin films. These materials have been used in a variety of transducers, which control current and convert either electrical or mechanical energy to the other or vice versa.

## 2.6 Lead Zirconate Titanate (PZT)

Even with the early success of barium titanate, mixed-oxide ceramics first dominated the ferroelectric field. In the early 1950s, ferroelectricity was discovered in lead zirconate titanate (PZT) with the chemical formula: $Pb(Ti_xZr_{1-x}O_3)$. The structure of PZT is a solid solution mixture of lead titanate ($PbTiO_3$) and lead zirconate ($PbZrO_3$). Importantly, PZT exhibits large piezoelectric coefficients around a morphotropic phase boundary (MPB), which literally means "the boundary between two forms", between tetragonal and rhombohedral ferroelectric phases. Near this boundary, which is controlled by composition, the crystal structure can change abruptly and its dielectric properties (both ferroelectric and piezoelectric) become anomalously large. For PZT, near the MPB the piezoelectric coefficient ($d_{33}$) can range from 200 to 750 pm/V depending on the dopants (Wada, Kakemoto, & Tsurumi, 2004). Its phase diagram was investigated and is shown below. The figure below illustrates some of the common uses of PZT-based piezoelectric materials (Bouzid, Bourim, Gabbay, & Fantozzi, 2005).

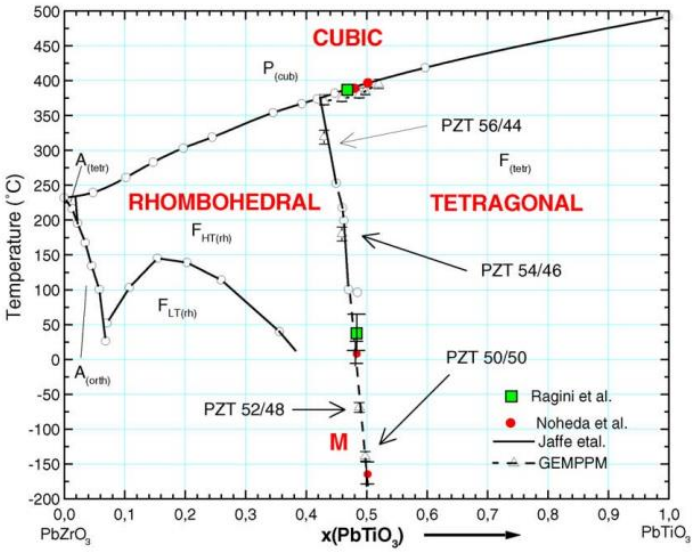


Figure 2.3 - Phase diagram for PZT showing different crystal structures **(Bouzid, Bourim, Gabbay, & Fantozzi, 2005)**

Currently, PZT is the most widely used piezoelectric ceramic material. It is used in a wide range of applications in the electroceramics field. There are two types of PZT: hard and soft. Hard PZT is used in sensors and high power ceramics that need to withstand high electrical voltage or mechanical stress, while soft PZT is used in actuators or when sensitivity is more important and the environmental conditions are not as destructive.

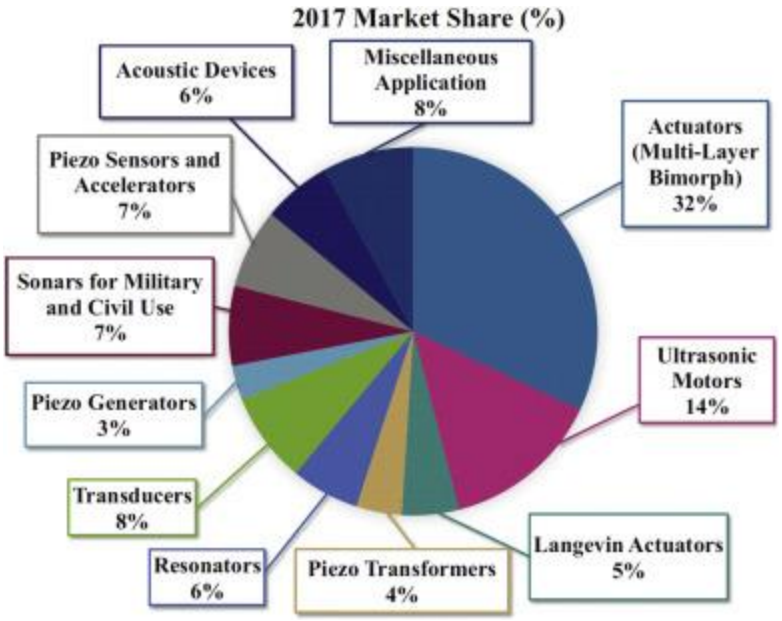


Figure 2.4 - Worldwide applications of piezoelectric materials **(Hong, et al., 2016)**

## 2.7 Ferroelectric Relaxors

After World War II, a young Soviet scientist from Yalta named Georgii Smolenski was investigating ferroelectric materials. Primarily, he focused on nonmetallic magnetic materials based on ferrites (The Great Soviet Encyclopedia (1979)). At the end of the 1940s, he discovered ferroelectric properties in lead titanate ($PbTiO_3$). Continuing to look at lead-based perovskites, he found an anomaly in the temperature coefficient of permittivity in lead zirconate ($PbZrO_3$). At the same time, perovskites with barium and strontium on the A-site also showed good ferroelectric behavior. Smolenski hypothesized that divalent A-site cations in perovskite-type materials are "ferroelectrically active". However, he struggled to replicate permittivity

measurements in other simple perovskite compounds. After accepting a position at the Institute for Chemistry of Silicates of the Academy of Sciences of the USSR, he began to experiment with complex perovskites. Complex perovskites incorporate charge compensation to maintain the overall $ABO_3$ stoichiometry.

In 1958, Smolenski and Agranovskaya (Smolenski & Agronovskaya, 1958) reported highly unusual dielectric behavior in complex perovskites with the general formula $Pb(X,Y)O_3$, where X and Y are both B-site cations of differing valence. Typically, X is a low valence cation (ex. $Ni^{2+}$) and Y is a high valence cation ($Nb^{5+}$). The first compounds investigated were $PbNi_{1/3}Nb_{2/3}O_3$ (PNN), and $PbMg_{1/3}Nb_{2/3}O_3$ (PMN). While common ferroelectrics have immediate phase transitions at the Curie temperature which can be observed in a simple permittivity measurement, these new materials exhibited diffuse phase transitions over large temperature ranges.

Recently, there has been a resurgence into the study of PNN due to its low dielectric maxima (-120°C) and improved synthesis abilities (Alberta & Bhalla, Low-Temperature Properties of Lead Nickel-Niobate Ceramics, 2002). The columbite precursor method is the preferred synthesis route for PNN. First, nickel niobate ($NiNb_2O_6$) is synthesized first to ensure a single phase final product without pyrochlore impurities. The nickel niobate is mixed and calcined before lead oxide (PbO) addition and then mixed and calcined again. The proper sintering temperature that maximizes the final product's dielectric constant and density is 1200°C for 2

hours for PNN. Data from XRD showed that PNN is a cubic perovskite with a lattice parameter of 4.025 Å.

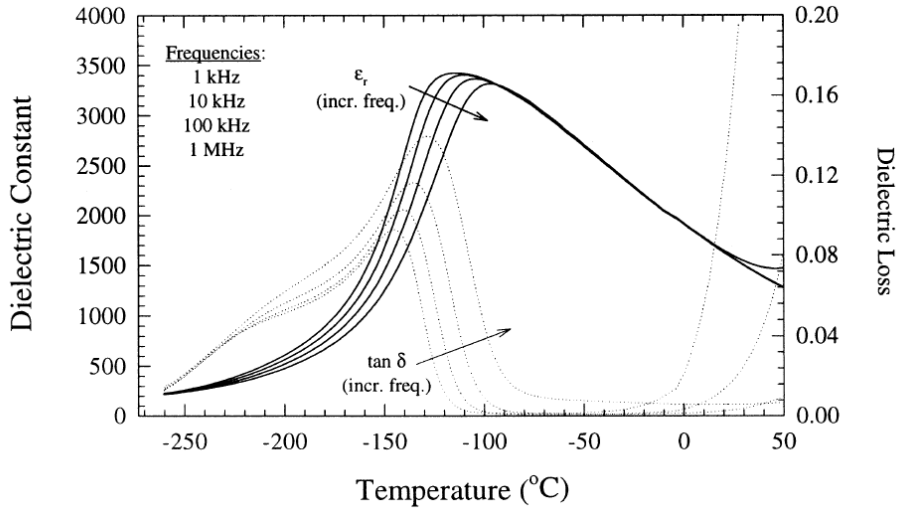


Figure 2.5 - low temperature dielectric data for PNN **(Alberta & Bhalla, Low-Temperature Properties of Lead Nickel-Niobate Ceramics, 2002)**

Shown above is a figure of the dielectric data of PNN. The graph clearly shows a diffuse phase transition over a large temperature range as typical in ferroelectric relaxors.

Single crystal lead magnesium niobate, $Pb(Mg_{1/3}Nb_{2/3})O_3$ (PMN) was one of the first relaxors studied alongside PNN in the late 1950s. Two Russian scientists named Vladimir Bokov and Irina Myl'nikova were the first to take electrical and optical measurements of PMN. They found that PMN is optically isotropic when cooled under applied field, but has remanent birefringence when the field is removed. In addition, ferroelectric domains can be observed under applied electric field, therefore the polarization of PMN crystals is due to domain motion like in classical

ferroelectrics. However, at low temperatures PMN exhibits non-ergodicity (Bokov & Myl'nikova, 1959). It can be an ideal material for applications which necessitate a low temperature diffuse phase transition due to its excellent dielectric broadening and low temperature permittivity maxima.

However, PMN can be difficult to synthesize using traditional solid solution synthesis which necessitates the use of a columbite method. In the method, an intermediate step to synthesize $MgNb_2O_6$ first is used to bypass the creation of a pyrochlore impurity phase and then mixed with PbO.

## 2.8 Relaxors Based on $BaTiO_3$-$Bi(Zn_{1/2}Ti_{1/2})O_3$ (BT-BZT)

The $BaTiO_3$-$Bi(Zn_{1/2}Ti_{1/2})O_3$ (BT-BZT) system has been studied extensively due to its smooth phase transition, relatively high permittivity, and high resistivity. The dielectric properties of BT can be changed and altered through doping or by creating homogenous solid solutions with analogous perovskite materials. It has been shown that BT-BZT is ideal for high density capacitors for energy storage applications. Primarily, the presence of paired barium and oxygen vacancies improves the insulation resistance of dielectrics (Raengthon, DeRose, Brennecka, & Cann, 2012).

The stoichiometric formula for the best electronic properties of polycrystalline BT-BZT in this system was with 2% Ba-deficient $(Ba_{0.78}\square_{0.02}Bi_{2.0})(Zn_{0.1}Ti_{0.9})O_{2.98}$. The system possesses a high relative permittivity along with low dielectric loss, ideal for linear dielectrics (Raengthon & Cann, 2011). Typically unstable, $Bi(Zn_{1/2}Ti_{1/2})O_3$

incorporated into a $BaTiO_3$ matrix creates a stable ceramic that exhibits dielectric relaxation characteristic of a ferroelectric relaxor. In relaxors, the temperature where permittivity is at a maximum ($T_{max}$) signifies the start of the phase transition. For BT-BZT, $T_{max}$ is located between 20°C – 190°C with a relative permittivity slightly above 1500 with low dielectric loss until 500°C. Below is a graph showing the temperature dependence of permittivity in the 80BT-20BZT system (Raengthon & Cann, 2011).

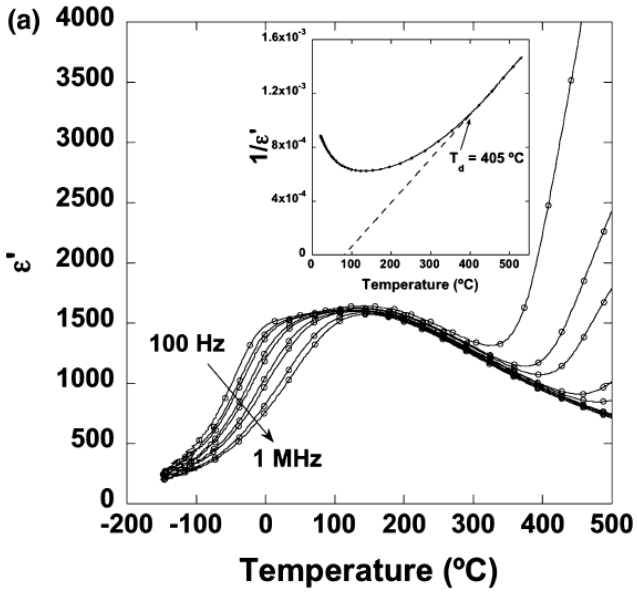


Figure 2.6 - Permittivity of $80BaTiO_3$-$20Bi(Zn_{1/2}Ti_{1/2})O_3$ from -150° to 500° **(Raengthon & Cann, 2011)**

While having interesting electronic properties, the BT-BZT system provides a framework for other interesting dopants in order to optimize the properties for demanding capacitor applications.

## 2.9 Relaxors Based on $BaTiO_3$-$Bi(Zn_{1/2}Ti_{1/2})O_3$-$BiScO_3$ (BT-BZT-BS)

Ceramics in the $BaTiO_3$-$Bi(Zn_{1/2}Ti_{1/2})O_3$-$BiScO_3$ system also exhibit excellent dielectric properties, creating a typical pseudocubic relaxor. They have been studied containing the following stoichiometries: $xBaTiO_3$-$(100-x)(0.5Bi(Zn_{1/2}Ti_{1/2})O_3$-$0.5BiScO_3)$ where x = 50, 55, and 60 (Raengthon, Sebastian, Cumming, Reaney, & Cann, 2012). These materials have a relatively high permittivity (K~1500), very low temperature coefficients of permittivity (TCε ~ 150), and $T_{max}$ near 100°C.

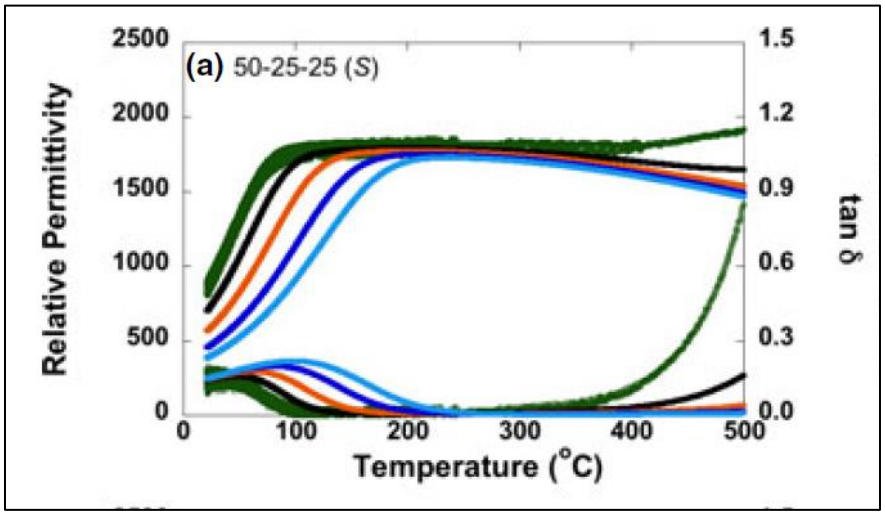


Figure 2.7 - Relative permittivity from room temperature to 500 °C for 50BT-25BZT-25BS **(Raengthon, Sebastian, Cumming, Reaney, & Cann, 2012)**

## 2.10 Relaxors Based on $BaTiO_3$-$Bi(Zn_{1/2}Ti_{1/2})O_3$-$NaNbO_3$ (BT-BZT-NN)

The $BaTiO_3$-$Bi(Zn_{1/2}Ti_{1/2})O_3$-$NaNbO_3$ (BT-BZT-NN) system has also been investigated with interesting results. Maintaining BZT and NN stoichiometry and decreasing the mole content of BT led to a broadening in the temperature-dependent permittivity (Raengthon, Brown-Shaklee, Brennecka, & Cann, 2013). In compositions where BZT was replaced by NN, the temperature of maximum permittivity was shifted to lower temperatures, the lowest being – 103 ºC for 70BT-5BZT-25NN. The entire ternary system shows promising dielectric properties. However, only compositions with BT > 50% were of single phase cubic symmetry. Overall, by increasing the BZT-NN concentration, the temperature stability of relative permittivity was improved, but the overall permittivity decreased and there was no change in temperature of maximum permittivity.

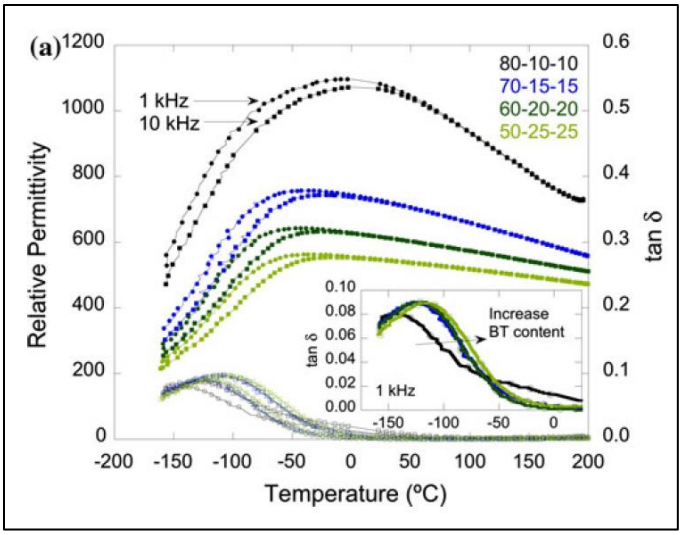


Figure 2.8 - Relative permittivity from -150 to 200 °C for the BT-BZT-NN system **(Raengthon, Brown-Shaklee, Brennecka, & Cann, 2013)**

## 2.11 Polar Nano Regions

Ferroelectric materials with relaxor behavior are almost exclusively observed in solid solutions with high cation disorder, which also makes characterization more difficult. Disorder can be finely tuned by precisely controlling stoichiometry, directly changing electronic and physical properties. The high degree of cation disorder is the underlying mechanism for the diffuse phase transition in relaxors. The disorder creates polar nano regions due to small fluctuations of dipole moments in the material (Viehland, Jang, Cross, & Wuttig, 1990). Induced dipoles in the structure can be characterized by their correlation length. The correlation length is a measurement of the ability of the dipole to respond in a correlated manner to an applied electric field. In a typical ferroelectric material, the correlation length is significantly larger than the

lattice parameter, i.e. the size of a unit cell, and strongly dependent on temperature, as seen in classic permittivity vs temperature measurements.

However, in relaxors, the correlation length is much smaller, leading to only small portions of the material's dipoles responding to outside influence, interfering with the natural long-range ordering of a typical ferroelectric. Essentially, polar nanoregions are microdomains embedded in a pre-existing framework and have a naturally lower symmetry than the surrounding system (Macutkevic, Banys, Bussman-Holder, & Bishop, 2011).

## 2.12 Temperature of Maximum Permittivity

In capacitor measurements, the temperature of maximum permittivity is an important material property ($T_{max}$). Ferroelectrics have a maximum permittivity at their Curie temperature, i.e. when the material goes through a phase change. A classical ferroelectric like PZT exhibits a drastic increase in permittivity near its Curie temperature. It can be difficult to unambiguously establish the Curie temperature of a relaxor due the presence of a diffuse phase transition. Instead, relaxors are characterized by the temperature at which the relative permittivity exhibits a maximum, $T_{max}$, which is usually frequency dependent.

## 2.13 Hysteresis Loops

Ferroelectric materials can be characterized by measuring their polarization ($P_i$) as a function of applied AC electric field ($E_j$). The polarization is governed by the equation:

$$P_i = \chi_{ij} E_j$$

where $P_i$ is the polarization vector ($C/m^2$), $\chi_{ij}$ is the dielectric susceptibility (f/m), and $E_j$ is the applied electric field (V/m). The application of an electric field on an insulating material polarizes the material by separating positive and negative charges, which is measured as the displacement field vector ($D_i$) or charge density. Ferroelectric materials will exhibit a characteristic hysteresis due to the movement of charge as the material changes from one polarization state to another. The displacement vector field vector is the total surface charge density induced on the material by the applied field and includes both the polarization of the material and the charges created by the polarization of free space and is defined as (Mayergoyz, 2005):

$$D_i = \varepsilon_0 E_i + P_i$$

For a typical ferroelectric material, P(E) measurement involve a hysteresis loop; an example of which is shown below for the material $42PbTiO_3$-$29BiScO_3$-$Bi(Mg_{0.5}Ti_{0.5})O_3$ (Figure1): (Ansell, Nikkel, Cann, & Sehirioglu, 2012).

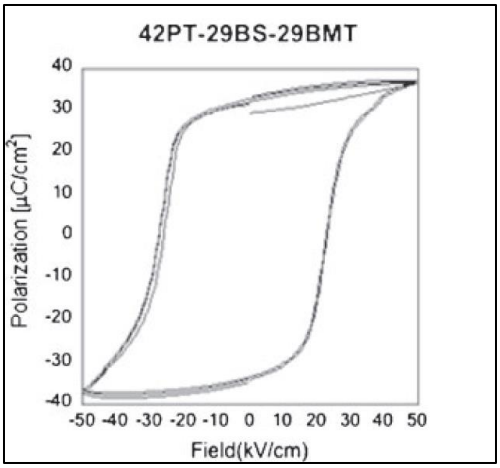


Figure 2.9 - Polarization vs. electric field for 42PT-29BS-29BMT at room temperature **(Ansell, Nikkel, Cann, & Sehirioglu, 2012)**

Adding in the equation (above) for the material polarization gives:

$$D_i = \varepsilon_0 E_i + P_i = \varepsilon_0 E_i + \chi_{ij} E_j = \varepsilon_0 \delta_{ij} E_j + \chi_{ij} E_j = E_i(\varepsilon_0 \delta_{ij} + \chi_{ij}) = \varepsilon_{ij} E_j$$

where $\varepsilon_{ij} = \varepsilon_0 \delta_{ij} + \chi_{ij}$ is the dielectric permittivity, $\delta_{ij}$ is Kronecker's symbol ($\delta_{ij} = 1$ for $i = j$, $\delta_{ij} = 0$ for $i \neq j$). Other types of materials respond differently under an applied electric field. The materials presented in this thesis are linear dielectrics, aptly named due to their linear polarization response to an electric field. An example of a P-E measurement on these materials is shown below (Figure 1):

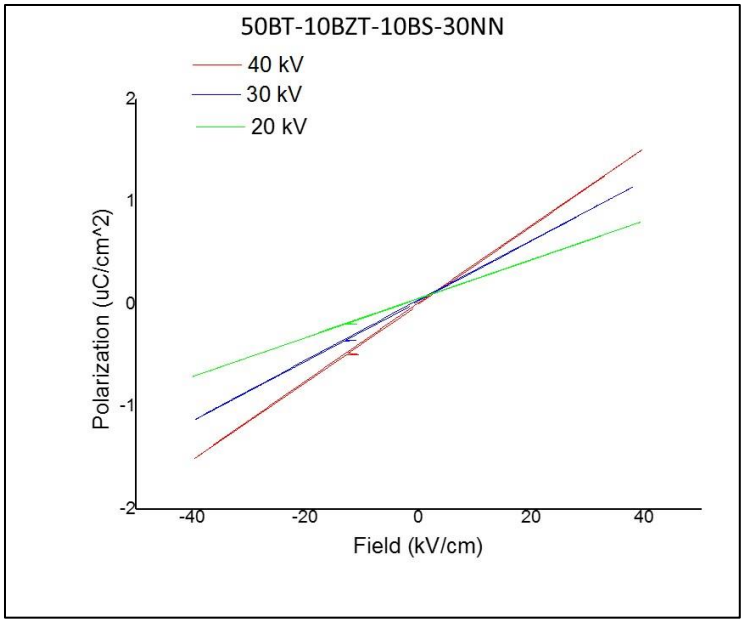


Figure 2.10 - Polarization vs. electric field for 50BT-10BZT-10BS-30NN at room temperature

Unlike linear dielectrics, relaxor materials have a non-linear slope when polarized. The slope of their polarization curve is a function of external electric field, and similar to linear dielectrics they also do not maintain their polarization once the electric field is removed, which is called remanent polarization. An example is shown below (Evans):

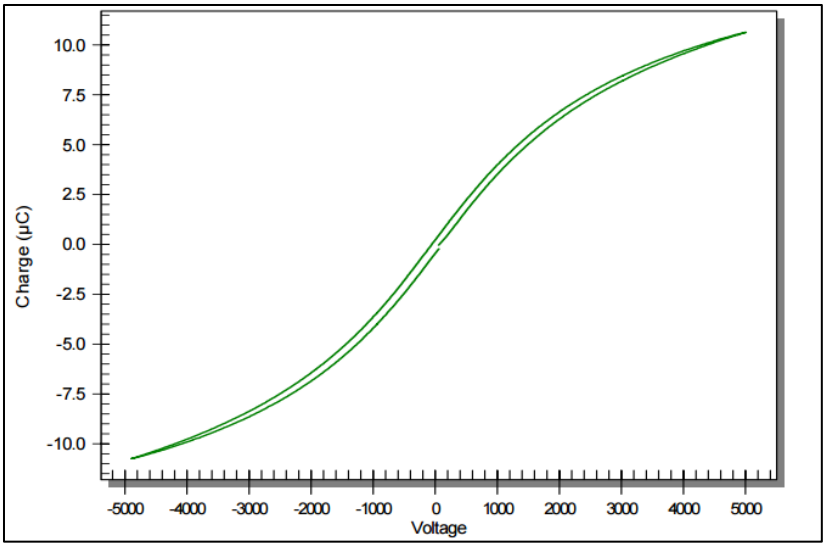


Figure 2.11 - Polarization vs. electric field for a high voltage paraelectric capacitor **(Evans)**

## 2.14 Ferroelectric Domains

Ferroelectric materials are characterized by a finite polarization in the absence of an external electric field. This polarization possesses two individually stable states that can be reversibly switched from one state to another by the application of an electric field. There can exist different regions in the material with different orientations due to the lack of homogenous polarization throughout polycrystalline ferroelectric ceramics. The regions of the crystal with uniformly oriented spontaneous polarizations are called ferroelectric domains, which can change and move under certain external stimuli.

The walls between domains of oppositely oriented polarization are called 180º domain walls, and walls separating perpendicularly oriented domains are called 90º

domain walls. The movement of domain walls and the orientation of domains have macroscopic effects that can be measured, resulting in phenomena such as a polarization hysteresis, aging, and fatigue. Caspari and Merz were the first to postulate that hysteresis is due to the presence of parallel and antiparallel domains switching at various field strengths (Caspari, 1950). The domain wall model was developed with the assumption that an applied external field produced an internal force against domains, causing them to re-orient direction.

Ferroelectric domains can be observed optically, as was first shown by Merz in 1954 and is shown below: (Merz W. , 1954)

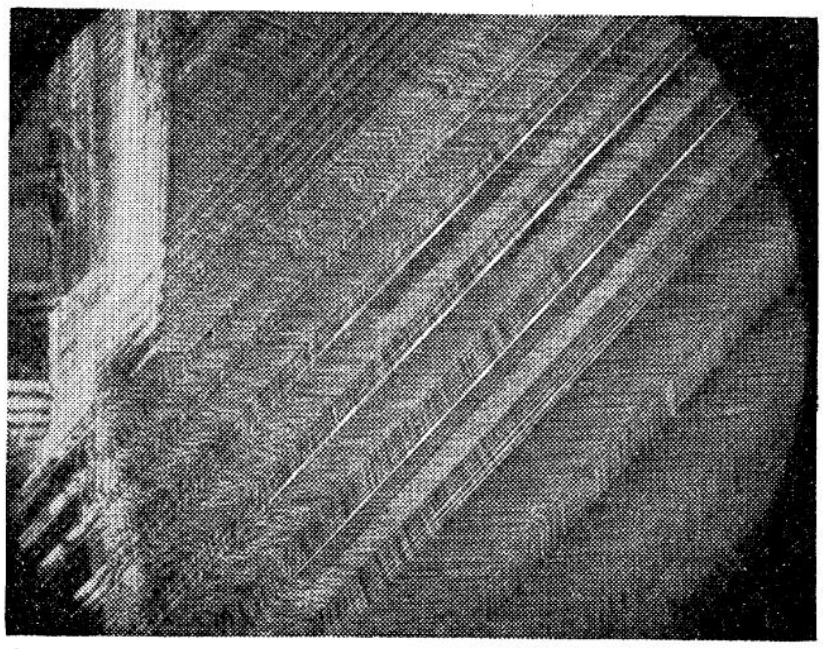

Figure 2.12 - 180° and 90° domains in single crystal $BaTiO_3$ **(Merz W. , 1954)**

Domain walls are naturally of lower symmetry than the host paraelectric phase of the material and can be thought of as functional, dynamic interfaces between areas of homogenous polarization. There are primarily two ways a material can change polarization under the influence of an electric field: either existing domain walls are bent or moved (i.e. $BaTiO_3$) or entirely new domains are formed as seen in magnetized iron.

## 2.15 Temperature Coefficient of Permittivity

The dielectric permittivity describes how much charge a medium can store from the induced movement of internal dipoles by an electric field. For most electroceramics, the permittivity is dependent on both frequency and temperature. The temperature coefficient of permittivity (TCε) is a mathematical means to quantify the effect of temperature on permittivity. Ferroelectrics can use TCε, but since they exhibit one or more phase transitions, the coefficient is insufficient to properly describe the temperature dependence of the dielectric properties. The equation for TCε is:

$$\mathrm{TC}\varepsilon = (\frac{1}{\varepsilon_b})(\frac{-(\epsilon_c - \epsilon_a)}{c - a})$$

In this arrangement, the TCε of a specific temperature range can be found by defining the permittivity at three temperatures (a, b, and c) where a – b = b – c. Essentially, the TCε gives a glimpse of the permittivity change over a specified temperature range (i.e. if TCε = 0, the dielectric properties are independent of temperature over the

range). If the temperature range contains $T_{max}$, the value of TCε will not correctly represent the response in the system. The units of TCε are part per million per degree Celsius.

## 2.16 Impedance Spectroscopy

There are two types of electrical current: direct current (DC) and alternating current (AC). Direct current is simple to understand: it is the constant, unidirectional flow of electrons creating an electric current. In a DC circuit, the opposition a current in material encounters is called resistance. As the magnitude of resistance increases, the more voltage is needed to create a current. DC theory is defined by Ohm's Law:

$$E = IR$$

where $E$ is the DC potential (V), $R$ is the resistance of the system (Ω), and $I$ is the resulting current (A). Alternating current, on the other hand, is the flow of electric current due to the periodical change of electric charge. An AC circuit also has similar property to resistance, called impedance, where a material resists the flow of electric charge. Impedance and resistance are both terms that denote the opposite to the flow of electrons. But the impedance also possesses both magnitude and phase shift due to AC signals having a frequency of oscillation. The figure below shows the phase shift (Breitkopf, 2012):

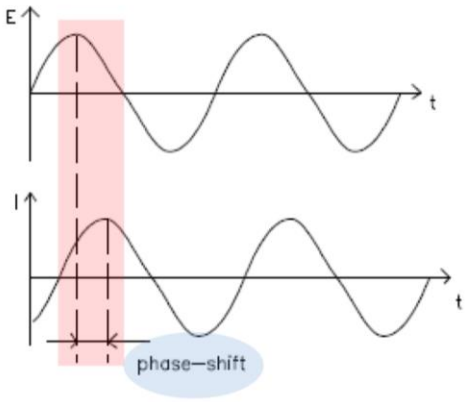


Figure 2.13 - Measured phase shift in impedance spectroscopy **(Breitkopf, 2012)**

Impedance possess two parts, a real and imaginary, so is most commonly presented as a complex number; resistance can be thought of as impedance with a 0º phase shift and therefore does not contain an imaginary representation. AC theory is defined by the analogous equation:

$$E = IZ$$

where $E$ is the DC potential (V), $Z$ is the impedance of the system (Ω), and $I$ is the resulting current (A). The excitation of the AC circuit, or the applied voltage, at any time is a sine function due to the existence of the phase angle shift:

$$E_t = E_o \sin(\omega t)$$

where $E_t$ is the potential at time t, $E_0$ is the amplitude, and ω is the radial frequency ($2\pi f$).

And the response from the circuit, or the current, at any time is also a sine function:

$$I_t = I_o \sin(\omega t + \phi)$$

where $I_t$ is the current at time t, $I_0$ is the amplitude, and $\phi$ is phase.

The most common form of impedance spectroscopy is the equivalent circuit measurement. The impedance of a capacitor has no real component, and its imaginary component is a function of both capacitance and frequency. Solving for Z produces:

$$Z = \frac{E_t}{I_t} = \frac{E_o \sin(\omega t)}{I_o \sin(\omega t + \phi)} = Z_0 \frac{\sin(\omega t)}{\sin(\omega t + \phi)}$$

where Z is the impedance and $Z_0$ is the magnitude. To represent impedance as a complex function, first the variable $j = \sqrt{-1}$ and using Euler's relationship, $\exp(j\phi) = \cos(\phi) + j\sin(\phi)$:

$$Z(\omega) = \frac{E_o \sin(j\omega t)}{I_o \sin(j\omega t + \phi)} = Z_0(cos\phi + jsin\phi)$$

To determine the total impedance of a combination of simple elements, the impedance of the individual components are summed according to equivalent circuit theory. For two circuit elements in series:

$$Z_{TOT} = Z_1 + Z_2$$

where $Z_1$ and $Z_2$ are the impedance of the elements. In complex number representation, the equation changes to:

$$(Z'_{TOT} + Z''_{TOT}) = (Z'_1 + Z''_1) + (Z'_2 + Z''_2)$$

The most popular form for representing impedance spectroscopy data is the Nyquist Plot. In this type of model, the imaginary impedance component (Z'') is plotted on the x-axis against the real impedance component (Z') on the y-axis. An example of

impedance spectroscopy using a Nyquist Plot on BT-BZT is shown below (Raengthon & Cann, 2011):

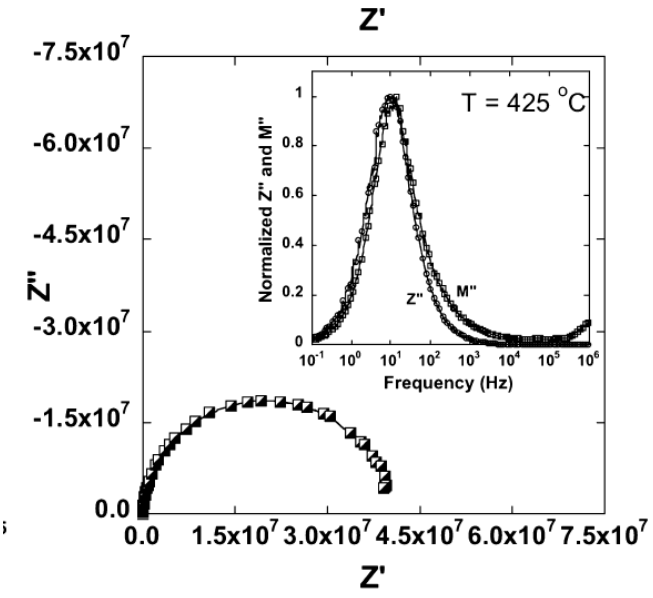


Figure 2.14 - Nyquist plot of impedance spectroscopy of 2% barium deficient $80BaTiO_3$-$20Bi(Zn_{1/2}Ti_{1/2})O_3$ **(Raengthon & Cann, 2011)**

Each point on the Nyquist plot is the impedance of the system at one frequency. It is represented as the vector from the origin to the point with length |Z|. The angle between the vector and x-axis is the phase angle. To obtain information from a Nyquist plot, one must first understand that the x-axis is the real and the y-axis is imaginary part of impedance, and that frequency increases along the x-axis. The plot of these points is a semicircle, and the number of semicircles corresponds to the number of time constraints of the system, indicative of differing relaxation times. Typically in polycrystalline materials, there are two semicircles: the high frequency semicircle, with lower resistance and closer to the origin, corresponds with crystalline

grains, and the low frequency semicircle, larger and more prominent and of higher resistance, corresponds to grain boundaries.

## 2.17 X-Ray Diffraction

The first major discovery of using X-rays to probe materials came from a one-page report titled: "The undersigned are engaged since 21 April 1912 with experiments about the interference of X-rays passing through crystals." It was signed by German physicist Walter Friedrich, Paul Knipping, and Max von Laue (Eckert, 2012). Within a year, English physicists father and son duo William Henry Bragg and William Lawrence Bragg developed an alternative method by which they confirmed the discovery. Immediately, the scientific community realized the importance of the new phenomena. Both von Laue and the Braggs would receive the Nobel Prize in 1914 and 1915, respectively. The equation governing diffraction is now called the Bragg's Law and is as follows:

$$2dsin\,\theta = n\lambda$$

where d is the spacing between diffracting planes (m), θ is the scattering angle (º), n is a positive integer, and λ is the wavelength of the incident wave (m). Bragg's Law connects the observed scattering with reflections from periodically spaced planes within a crystal structure. This interaction is a form of elastic scattering: incoming X-rays have the same energy and wavelength as outgoing X-rays. Diffraction only occurs when *n* is an integer value, thereby fulfilling the requirements of Bragg's Law.

The diffraction pattern of a sample can be characterized by applying Bragg's law to the angle between diffracting planes to find the d-spacing, the physical length, between atoms in the crystal.

The intensity of each reflection of miller indices *hkl* is proportional to the squared structure factor in three dimensional space: $I_{hkl} \sim |F_{hkl}|^2$. However, the total intensity of a diffraction peak is defined as:

$$I_{hkl} = |F_{hkl}|^2 \; x \; M_{hkl} \; x \; LP\theta \; x \; TF\theta \; x \; A\theta$$

where $F_{hkl}$ is the structure factor, $M_{hkl}$ is the multiplicity, $LP\theta$ is the Lorentz-polarization correction, $TF\theta$ is the temperature factor, and $A\theta$ is the absorption factor.

The structure factor is a complex number and is defined as the Fourier transformation of the electron density in the unit cell:

$$F_{hkl} = \sum_j \iiint \rho(xyz) \exp[2\pi i(hx + ky + lz)] \, dxdydz$$

where ρ(xyz) is the electron density tripled integrated over the volume of a single atom, and so the summation is over all atoms in the unit cell. It can be assumed that all atoms of a specific type have similar electron distributions, and since X-ray scattering is due to all the electrons in an atom, any variations from bonding or differing valence states will be negligible. Thus, atoms will react similarly regardless of system, so numerical values found by experimental quantum mechanics can be given to each type of atom. This numerical value is called the atomic scattering factor, and is denoted by the letter *f*. The previous equation can be re-written as:

$$F_{hkl} = \sum_j f_j \exp[\, 2\pi i\left(hx_j + ky_j + lz_j\right)]$$

Multiplicity comes from symmetry and describes the number of equivalent d-spacings for related reflections. Lower symmetry configurations will have lower multiplicities. For example: in a cubic crystal structure, *a* =*b* = *c*, so the planes (100), (010), (001), (-100), (0-10), and (00-1) all have the same d-spacing and a multiplicity of six.

The Lorentz-polarization correction is a combination of two geometric corrections: the Lorentz factor and polarization factor. X-rays are electromagnetic radiation, and so are scattered with an amplitude proportional to the sine of the angle between the incident radiation and the scattering angle. Since the incident beam is not polarized, the X-rays can scatter differently based on the angle between the beam and electric field will differ. The polarization factor corrects for this possibility.

The Lorentz factor comes from the fact that crystals can still diffract at angles that slightly different than their predicted Bragg angle and lower angles tend to have artificially increased intensities due to higher angles taking more time to diffract.

Typically, these two geometric corrections are combined. Together, they decrease the intensity of reflections at intermediate angles relative to those at low and high angles. The Lorentz-polarization correction is:

$$LP\theta = \frac{1 + cos^2 2\theta}{(sin^2\theta cos\theta)}$$

Atoms in a crystal structure can undergo thermal vibrations when under the influence of electromagnetic radiation. In response, diffraction data will be inconsistent due to unit cell oscillations, the overall intensity of diffraction lines will decrease, and the background scattering will increase. The Temperature Factor addresses these problems and is defined as:

$$TF\theta = \exp[-B\frac{sin^2\theta}{\lambda^2}]$$

where B is the isotropic temperature factor which is proportional to the mean squared displacement of the atoms and changes depending on the system and λ is the wavelength of incident light.

Atoms can absorb incident photons, and this can reduce the intensity of diffraction. Typically atoms with higher atomic number absorb some X-rays rather than scatter. The observed intensity I is given by:

$$I = I_0 \exp(-\mu x)$$

where $I_0$ is the true intensity, μ is the linear absorption coefficient, and *x* is the total path length.

Diffraction patterns describe the physical arrangement of atoms in the unit cell and their symmetry. At first, only simple structures could be mapped: as experiments improved, deducing atomic positions for three dimensional crystals became a viable scientific technique. The realm of x-ray diffraction expanded due to its many uses. In minerology and metallurgy, the technique is often used to examine the chemical

makeup of unknown solids. These concepts of diffraction were also applied to neutron diffraction and electron diffraction.

## 2.18 Electron Microprobe Analysis

A very common technique in geology and materials science is electron microprobe analysis (EPMA), which is an analytical tool to determine the chemical composition of a solid sample. This is typically used to characterize rocks based on the differing amounts of elements present in their framework. A beam of electrons is fired at the sample in vacuum using a tungsten filament. The electrons hit the material, knocking inner orbital electrons out of the system, creating an energy difference that allows for outer electrons to relax. The relaxation of an outer electron emits a characteristic X-ray which is identified by the detector. This technique is not often used on ceramics due to their surface roughness and porosity but were investigated using the EPMA in the Earth, Ocean, and Atmospheric Sciences at Oregon State.

## 2.19 Capacitor Classification

The goals of this project are dictated by the Internal Electrotechnical Commission (IEC) to create a capacitor that fulfills the required government classifications. The IEC has created three classes of ceramic capacitors: Class 1, high stability and low losses for resonant circuit applications; Class 2, high volumetric efficiency for smoothing, by-pass, coupling, and decoupling applications; and Class 3, barrier layer

capacitors. A Class 1 ceramic capacitor (i.e. $MgNb_2O_6$) is characterized by low relative permittivity due to low volumetric efficiency (below 50), but have a TCε of nearly zero. Class 2 capacitors offer high dielectric constants but low accuracy and stability and are typically made of single phase ferroelectric materials. Class 3 capacitors exhibit barrier layers and have very high permittivity (up to 50,000) but offer little accuracy and stability. The permittivity over any temperature range is nonlinear and so Class 2 capacitors are not suited for precision and are typically made of doped ferroelectric materials.

The capacitors presented in this thesis are Class 2 ceramic capacitors. There is a coding system to further classify these capacitors consisting of a letter, a number, and a letter. Each character corresponds to a numerical number: first letter gives the low temperature limit, the number gives the high temperature limit, and the last letter gives the change in capacity over the temperature range required for the classification. The lower temperature letter codes are: X = -55 Cº, Y = -30 Cº, and Z = +10 Cº; the upper temperature number codes are: 4= +65 Cº, 5 = +85 Cº, 6 = +105 Cº, 7 = +125 Cº, 8 = +150 Cº, and 9 = +200 Cº; the letter code for the percentage change in capacity over the given temperature range is: P = ±10%, R = ±15%, P = ±10%, S = ±22%, T = +22/-32%, U = +22/-56%, V = +22/-82%. Ideal products from this project are Class 2 capacitors with classifications: X7R, only a 15% change in capacitance between -55 – +125 Cº; Y5V, a capacitance somewhere between +22%

and -82% between -30 – +85 Cº; and X9R, only a 15% change in capacitance between -55 – +200 Cº (Multilayer Ceramic Capacitors/Axial & Radial Leaded).

## 2.20 Statement of Objective

Linear dielectrics with temperature-stable electronic properties are necessary for continued technological innovation. The goal of this project is to create high voltage ceramic capacitors with (1) temperature of max permittivity below room temperature, (2) a temperature coefficient of permittivity near zero, and (3) an overall high relative permittivity to have practical application. In this study, three solid-solution ferroelectric systems were investigated: $BaTiO_3$-$Bi(Zn_{1/2}Ti_{1/2})O_3$-$BiScO_3$-$NaNbO_3$, $BaTiO_3$-$Bi(Zn_{1/2}Ti_{1/2})O_3$-$Pb(Mg_{1/3}Nb_{2/3})O_3$, and $BaTiO_3$-$Bi(Zn_{1/2}Ti_{1/2})O_3$-$Pb(Ni_{1/3}Nb_{2/3})O_3$. Previous research suggests that these are ideal candidates for creating a dielectric material with a diffuse ferroelectric-to-relaxor phase transition, allowing for similar electronic properties over a wide range of temperatures.

# Chapter 3 – Materials and Methods

This chapter presents the experimental details on the planning, design, and execution to synthesize and measure the dielectric and ferroelectric properties of BT-BZT-BS-NN, BT-BZT-PNN, and BT-BZT-PMN ceramics. The experiments were designed using the standard ceramic synthesis techniques with alterations based on composition.

Widely known as a useful non-lead ferroelectric, $BaTiO_3$ was used as the majority constituent due to its excellent electronic properties, and other perovskite ferroelectric compounds were introduced into the system to attempt to synthesize a relaxor with high B-site disorder. Studies have shown that stoichiometric $Bi(Zn_{1/2}Ti_{1/2})O_3$-$BiScO_3$ addition into an existing BT system reduces the temperature coefficient of permittivity. To shift the maximum permittivity down, also lowering the operating range and ferroelectric phase transition, $NaNbO_3$ was utilized; however, it has naturally lower relative permittivity. This quaternary system builds upon previous research based on the BT-BZT, BT-BZT-BS, and BT-BZT-NN systems previously discussed in this thesis.

The first step was to create an ideal synthesis route. All samples were prepared using the solid state technique. The powders were mixed and calcined at 900 °C and sintering temperatures ranged from 1100 °C to 1200 °C. Multiple

characterization techniques were used to examine physical and electronic properties to confirm single phase relaxor devices. A single phase material is necessary for reproducible results and predictable material properties.

These relaxors are ideal for capacitor applications due to their highly diffuse phase transition. At the temperature of maximum permittivity, the lattice changes from tetragonal symmetry to cubic symmetry. In typical ferroelectrics, this is called the Curie temperature and is accompanied by a peak in permittivity. In relaxors, there is no Curie temperature: instead, the material gradually changes physical structure over a large temperature range, as seen by a broad permittivity peak. Characterizing the symmetry of relaxors can be difficult due to their diffuse phase transition: in these types of material, long-range structure is pseudocubic, while local structure is non-cubic. It is important to understand the physical lattice structure because of its direct effect on electronic properties. X-ray diffraction allows for symmetry information to be collected and was performed on all samples twice; after calcining and after sintering. If a composition of mixed phase was obtained after calcination, the material was discarded as a possible dielectric. In this manner, only the dielectric properties of the best compositions were investigated. Compositions of high atomic percent BT were the first materials made in this study but exhibited poor temperature-dependent properties. With each new batch, the atomic percent of BT was lowered, BZT while equal BZT-BS stoichiometry was maintained.

## 3.1 Synthesis of $BaTiO_3$-$Bi(Zn_{1/2}Ti_{1/2})O_3$-$BiScO_3$-$NaNbO_3$

In this study, solid solutions of $BaTiO_3$-$Bi(Zn_{1/2}Ti_{1/2})O_3$-$BiScO_3$-$NaNbO_3$ (BT-BZT-BS-NN) have been prepared by a conventional solid-state method. Precursor powders of $BaCO_3$ (>99.8%), $Bi_2O_3$ (>99.99%), $Na_2CO_3$ (>99.95 %), $TiO_2$ (>99.9), ZnO (>99.9%), $Sc_2O_3$ (>99.995%), and $Nb_2O_5$ (>99.9%) were used as starting material. Prior to synthesis, $BaCO_3$ and $Na_2CO_3$ were dried for at least 24 hours and kept in a desiccator to remove water. The powders were weighed in appropriate stoichiometric amounts, dissolved in 100% ethanol, vibratory milled for 6 hours with zirconia media, and finally dried in a 75 °C oven overnight.

All powders were calcined in covered crucibles at different temperatures and XRD data was used to find the optimal temperature to produce single phase perovskites, which was found to be at least 900 °C for all compositions. This follows previous experimental data and is the same calcination temperature for BT-BZT compounds. The samples were calcined for 6 hours with a ramp rate of 10°C/min. After XRD, the powders were vibratory milled again for 6 hours and dried overnight in a 75 °C oven.

The phase-pure calcined powders were mixed with 3% by weight polyvinyl butyral binder (B-98 polyvinyl butyral resin by Solutia) and compressed into pellets under 3 metric tons of pressure for 2 minutes. Sintering regiments followed a similar pattern; the pellets were heated to 400 °C for 4 hours for binder burnout and then

heated to the sintering temperature and held for 6 hours, then brought back to room temperature with all oven temperature changes at a ramp rate of 5°C/min.

## 3.2 Synthesis of $BaTiO_3$-$Bi(Zn_{1/2}Ti_{1/2})O_3$-$Pb(Ni_{1/3}Nb_{2/3})O_3$

In this study, solid solutions of $BaTiO_3$-$Bi(Zn_{1/2}Ti_{1/2})O_3$-$Pb(Ni_{1/3}Nb_{2/3})O_3$ (BT-BZT-PNN) have been prepared by the conventional columbite solid-state method (Alberta & Bhalla, Low-temperature Properties of Lead Nickel-Niobate Ceramics, 2002). For PNN based compositions, powders of $Bi_2O_3$ (>99.99%), ZnO (>99.9%), $Nb_2O_5$ (>99.9%), $TiO_2$ (>99.9), $BaCO_3$ (>99.8%), PbO (>99.9%), and No (>99.9%) were used as starting material. First, precursors NiO and $Nb_2O_5$ were weighed in appropriate stoichiometric amounts, dissolved in 100% ethanol, vibratory milled for 12 hours with zirconia media, and finally dried in a 75 °C oven overnight. After drying, the solid solutions were calcined at 950 ºC for 3 hours in a closed crucible. Finally, the calcined powder is milled once again for 6 hours to reduce particle size and dried overnight.

The finished product, $NiNb_2O_6$, was mixed with PbO in stoichiometric amounts to form $Pb(Ni_{1/3}Nb_{2/3})O_3$. The mixture was mixed and milled for 24 hours with zirconia media. After drying, the solutions were calcined at 950 °C for 4 hours. The other precursors were weighed and added to the PNN powder and milled for 6 hours to create solid solutions of BT-BZT-PNN. After drying overnight, the finished

powder was calcined for a third time at temperatures ranging from 900 °C - 1000 °C for 3 hours. Single phases were confirmed using X-Ray diffraction.

The phase-pure calcined powders were mixed with 3% by weight polyvinyl butyral binder and compressed into pellets under 3 metric tons of pressure for 2 minutes. Sintering temperatures ranged from 1050 °C – 1150 °C all at a ramp rate of 5°C/min.

## 3.3 Synthesis of $BaTiO_3$-$Bi(Zn_{1/2}Ti_{1/2})O_3$-$Pb(Mg_{1/3}Nb_{2/3})O_3$

In this study, solid solutions of $BaTiO_3$-$Bi(Zn_{1/2}Ti_{1/2})O_3$-$Pb(Mg_{1/3}Nb_{2/3})O_3$ (BT-BZT-PMN) have been prepared by the conventional columbite solid-state method (Wongmaneerung, Sarakonsir, Yimnirun, & Ananta, 2006). Powders of $Bi_2O_3$ (>99.99%), ZnO (>99.9%), $Nb_2O_5$ (>99.9%), $TiO_2$ (>99.9), $BaCO_3$ (>99.8%), PbO (>99.9%), and MgO (>99.9%) were used as starting material. First, precursors MgO and $Ni_2O_5$ were weighed in appropriate stoichiometric amounts, dissolved in 100% ethanol, vibratory milled for 12 hours with zirconia media, and finally dried in a 75 °C oven overnight. After drying, the solid solutions were calcined at 1000 ºC for 4 hours in a closed crucible.

The $MgNb_2O_5$ precursor was mixed with PbO in stoichiometric amounts to form $Pb(Mg_{1/3}Nb_{2/3})O_3$ by mixing and milling for 24 hours with zirconia media. After drying, the solutions were calcined at 1000 °C for 4 hours. The mixed powders were mixed with the other precursors and milled for 6 hours to create solid solutions BT-

BZT-PMN. The finished powdered were calcined at temperatures ranging from 900 °C - 1000 °C for 3 hours. Single phase perovskite was confirmed using XRD.

The phase-pure calcined powders were mixed with 3% by weight polyvinyl butyral binder and compressed into pellets under 3 metric tons of pressure for 2 minutes. Sintering temperatures ranged from 1200 °C - 1250 °C with a ramp rate of 5°C/min.

## 3.4 Electronic Characterization

Once ceramic pellets were synthesized, they went through various testing. In order to measure the capacitance of the ceramic pellet samples, they need to be prepared in a parallel plate capacitor arrangement. After sintering, the samples were polished to create a smooth surface for adhesion. Silver electrodes were applied onto the parallel surfaces by painting a conductor paste on both sides and placed in a drying oven. After drying, the electrodes were fired at 700 °C with a 10 °C/min ramp rate for thirty minutes and sanded down to create a flat surface. A linear dielectric material can be confirmed by measuring its polarization (P) as a function of applied electric field (E). Typical ferroelectrics have a non-linear hysteresis loop in P(E) measurements: however, since these are relaxor dielectrics, the P-E response was found to be exactly linear.

Another way to characterize ferroelectrics is to measure their relative permittivity as a function of temperature. The pellets were placed into a NorECS

Probostat high-temperature measurement cell for dielectric measurements. The temperature dependence of permittivity was measured up to 550 °C with a 2 °C/min ramp rate using an Agilent 4284A LCR Meter and scanned in the frequency domain from 1Hz to 1MHz. Low temperature data (using liquid nitrogen) was taken from -50 °C to 125 °C with a 2 °C/min ramp rate.

## 3.5 Physical Characterization

To determine the samples physical structure, calcined powder and crushed sintered pellets were examined using X-Ray diffraction to confirm single phase perovskites.

Density measurements were taken using Archimedes' method; pellets were weighed in air, then placed into water on high heat for 8 hours. The water comes to a light boil, so refilling is necessary every 2 hours, and then the pellets were weighed in water. Knowing the sample weight in water and air and the densities of water and air at specific temperatures, the density can be calculated. When an object floats in a liquid, its upward buoyant force ($F_B$) is equal to the downward gravitational force ($m_0 g$). Once fully submerged, the buoyant force from the surrounding fluids acts on the object with an upward direction and magnitude equal to the weight of the fluid displaced by the object, which is the same as the density of the liquid ($\rho_L$) times the volume of fluid displaced ($V_L$).

$$F_B = m_0 g = \rho_L V_L$$

In this study, water and air were used as the fluids. For a solid body of volume V that is heavier than water, the buoyant force is:

$$F_B = \rho_w V g$$

The mass of the body M weighed in air is:

$$M_{air} = \rho V$$

So the volume of the object is equal to:

$$V = \frac{M_{air}}{\rho}$$

The weight of the body in air is the actual weight, and any differences in weight measurements can be attributed to the buoyant force acting on the body. The relationship between weights and buoyant force is shown below:

$$weight_{water} = weight_{air} - F_B$$

The weight of the body in water is the mass in water ($M_W$) multiplied by gravity, Plugging in, the equation becomes:

$$M_W g = M_{air} - \rho_w V g$$

and simplifying reduces to:

$$\rho = \frac{M_{air}\rho_w}{M_{air} - M_{water}}$$

Therefore, by measuring the weight in air and in water and by knowing the density of air and water (which is a function of temperature), the density of the body can be determined (Bengisu). For Archimedes measurements, sintered ceramic pellets are weighed in air, then placed in a mixing water bath for 8 hours at boil (water is added

as needed). The pellets are then moved to a scale that can weigh objects in water. Typically, three pellets per composition were used to minimize random errors in determining the density.

Typical ceramic density values are based off their accuracy to theoretical densities found using X-ray diffraction data. The most common way to determine theoretical density of a cubic unit cell is a combination of Cohen's method and the least squares method. Recall Bragg's Law:

$$\lambda = 2dsin\theta$$

Square the equation and plug in the formula for d-spacing:

$$d_{hkl} = \frac{a_0}{\sqrt{h^2 + k^2 + l^2}}$$

$$\lambda^2 = 4d^2sin^2\theta$$

Which becomes:

$$\lambda^2 = 4d^2sin^2\theta = \frac{4a_0^2}{(h^2 + k^2 + l^2)}\ sin^2\theta$$

And rearrange to solve for $\sin^2\theta$ :

$$sin^2\theta = (h^2 + k^2 + l^2)\frac{\lambda^2}{4a_0^2}$$

Since the wavelength ($\lambda$) and lattice vector ($a_0$) are constants, and $h^2 + k^2 + l^2$ must be an integer, the diffraction pattern of a sample can be correctly indexed for any given angle. To find the lattice parameter $a_0$, take the logarithmic of the square Bragg's Law:

$$\log(\lambda^2) = \log(4d^2 sin^2\theta)$$

Rearrange and reduce:

$$\log(sin^2\theta) = \log\left(\frac{\lambda^2}{4}\right) - \log(d)$$

After differentiation:

$$\frac{\Delta sin^2\theta}{sin^2\theta} = -\frac{2\Delta \mathrm{d}}{d}$$

Assuming that systemic errors are in the form:

$$\frac{2\Delta \mathrm{d}}{d} = Kcos^2\theta$$

Substitute back into the equation to give:

$$\frac{\Delta sin^2\theta}{sin^2\theta} = -2Kcos^2\theta$$

Combining equations:

$$\Delta sin^2\theta = -2Kcos^2\theta = Dsin^2\theta$$

Where D is a constant. To find the true lattice parameter:

$$sin^2\theta_{observed} - sin^2\theta_{true} = -\Delta sin^2\theta$$

Plugging in from the equation above where $\sin^2\theta$ was solved:

$$sin^2\theta_{observed} - (h^2 + k^2 + l^2)\frac{\lambda^2}{4a_0^2} = Dsin^2\theta$$

Which is simplified to:

$$sin^2\theta_{observed} = A\alpha + C\delta$$

Where A = $\frac{\lambda^2}{4a_0^2}$ , $\alpha = (h^2 + k^2 + l^2)$, C = D/10, and $\delta$ = 10sin$^2$2θ. By indexing the diffraction pattern, sin$^2$θ, $\alpha$, and $\delta$ are known, so A and C are determined by solved simultaneous equations for the observed reflections so the true value of the lattice parameter can be calculated. The presented value is the percent measured density compared to the theoretical density.

# Chapter 4 – Results

## 4.1 Quaternary System

The lead-free solid solution $BaTiO_3$-$Bi(Zn_{1/2}Ti_{1/2})O_3$-$BiScO_3$-$NaNbO_3$ (BT-BZT-BS-NN) was investigated as a possible low-temperature dielectric for capacitor application. Desirable traits of an ideal material consist of: temperature-stable permittivity so the capacitor can operate over a wide temperature range; a maximum permittivity below 0 °C; and a relative permittivity as high as possible, hopefully near 1000, to allow for practical use.

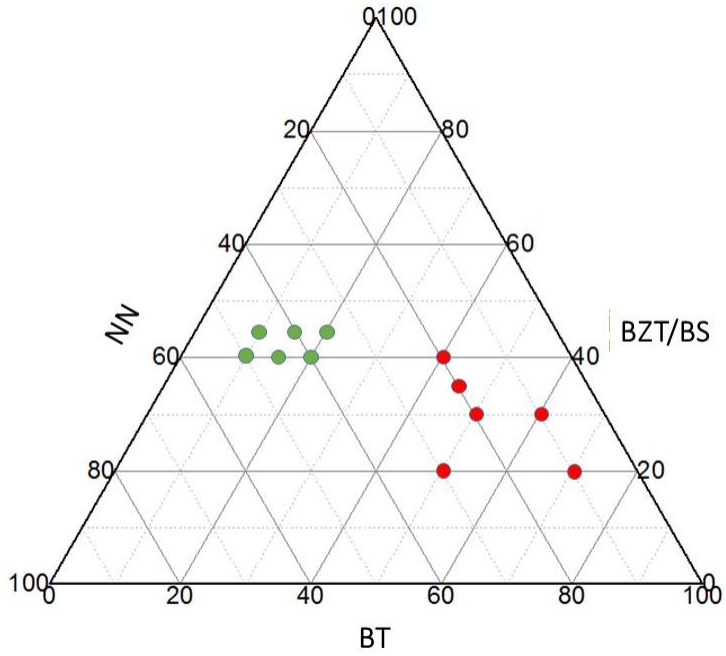


Figure 4.1 – $BaTiO_3$-$Bi(Zn_{1/2}Ti_{1/2})O_3$–$BiScO_3$–$NaNbO_3$ phase diagram; red compositions are single phase; green compositions are of mixed phase

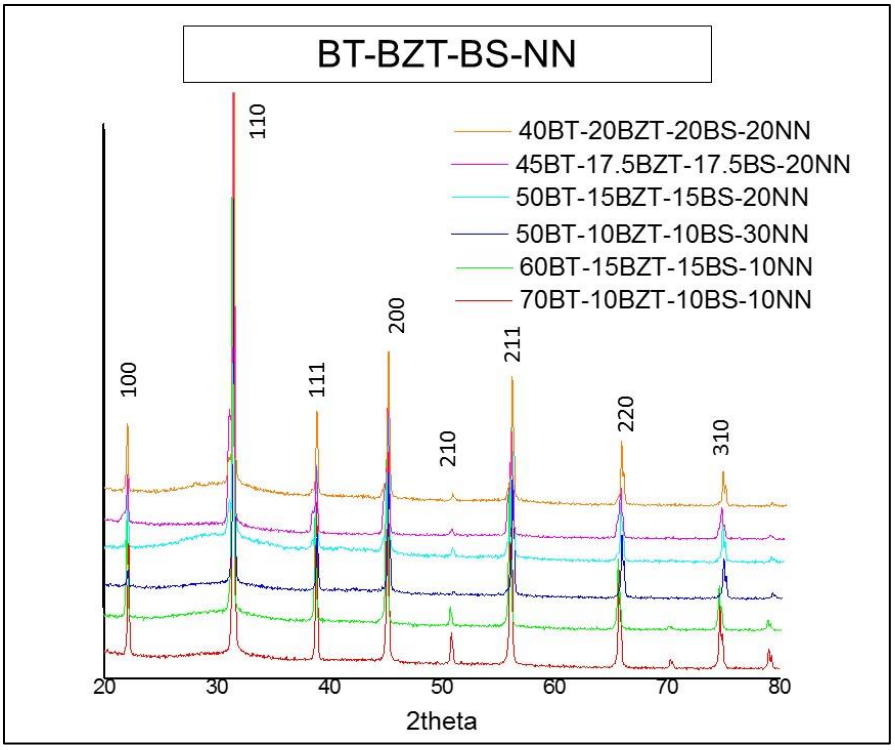


Figure 4.2 - X-ray diffraction profiles of single phase compositions

### 4.1.1 Physical Properties

X-ray diffraction (XRD) data of single phase material is shown in Figure 3.2. Depending on the temperature of maximum permittivity ($T_{max}$) and due to natural relaxor behavior, the compositions exhibit a mixture of tetragonal and cubic symmetry. However, $T_{max}$ can affect XRD results. For example: 50BT-10BZT-10BS-30NN has the lowest maximum permittivity at -27.5 °C. Performing XRD characterization at room temperature shows a singlet (200) peak, suggesting a pseudo-cubic unit cell at room temperature. The rest of the compositions have $T_{max}$

near or above RT, signifying that they are still tetragonal, and so the splitting of (200) peak is prominent.

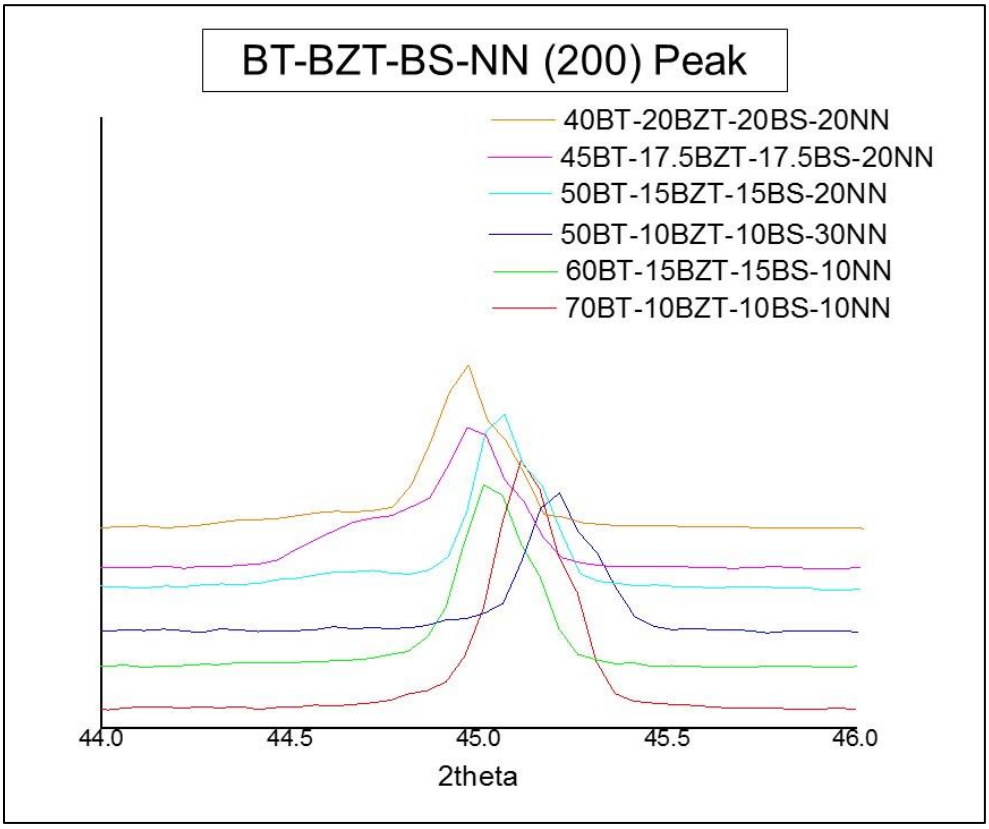


Figure 4.3 – BT-BZT-BS-NN (200) peak splitting

The theoretical densities were calculated once the lattice parameter was found using Cohen's method on the XRD data, shown in Table 4.1. Measured densities were found by Archimedes method and is often displayed as a percentage of theoretical density. Proper sintering temperatures ranged between 1100 °C and 1200 °C and are listed in Appendix A. The tolerance factor was calculated based on ionic radii from Shannon and Prewitt (Shannon, 1976).

Table 4.1 – Physical Properties of BT-BZT-BS-NN

| Composition | Lattice Parameter (Å) | Theoretical Density($g/cm^3$) | Measured Density ($g/cm^3$) | Tolerance Factor |
|---|---|---|---|---|
| 70BT-10BZT-10BS-10NN | 4.0165 | 6.18 | 5.93 | 1.0249 |
| 60BT-15BZT-15BS-10NN | 4.0247 | 6.33 | 6.14 | 1.0114 |
| 50BT-10BZT-10BS-30NN | 4.0160 | 5.83 | 5.64 | 1.0060 |
| 50BT-15BZT-15BS-20NN | 4.0219 | 6.17 | 5.96 | 1.0019 |
| 45BT-17.5BZT-17.5BS-20NN | 4.0269 | 6.24 | - | 0.9951 |
| 40BT-20BZT-20BS-20NN | 4.0297 | 6.32 | - | 0.9883 |

### 4.1.2 Electron Microprobe Analysis

The electronic and mechanical properties of the ferroelectric relaxors studied in this thesis are directly related to sample composition. The problem with ceramic pellets is that there is no easy way to identify element composition once synthesis is complete. Electron probe microanalysis (EPMA) is a common characterization technique used to determine the composition of a solid sample.

By using EPMA the pellets of differing compositions were examined and compared. The most important elements to confirm are the volatiles that can be lost during processing (e.g. Na), therefore changing the composition of the final sintered ceramic. Sintered ceramic pellets were compared against their initial stoichiometry, which is known, and to that of the other pellets in the system. The EPMA also has an electron microscope attached which was used to generate the micrograph shown in Fig. 4.4 below.

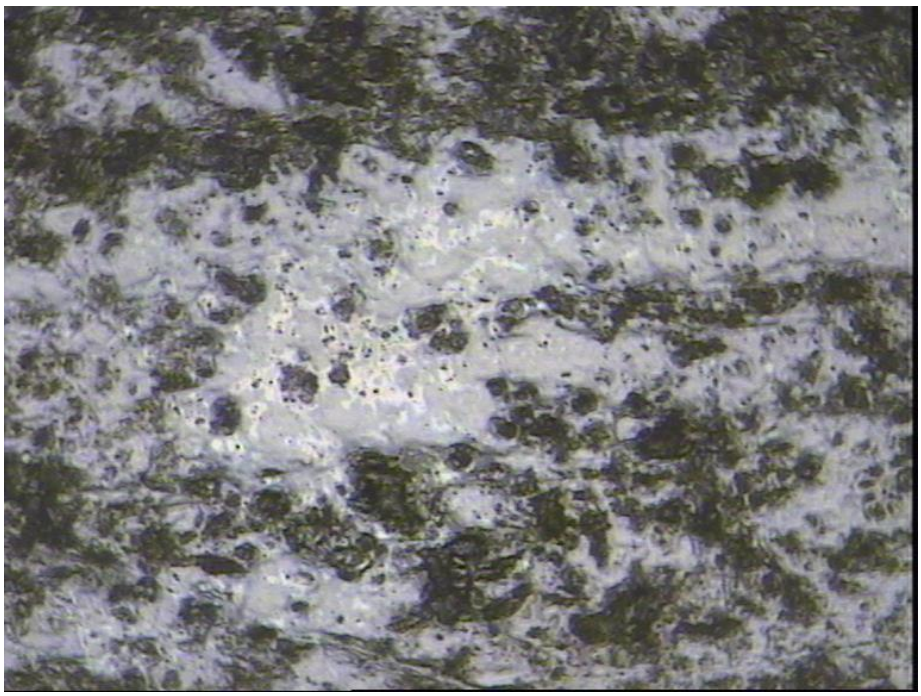

Figure 4.4 - Backscatter Electron (BSE) image of 50BT-10BZT-10BS-30NN pellet

The conditions used for the EPMA on the samples in this study were: instrument at 30 nA and 15 kV, beam size of 5 μm, which was large to account for poor samples. The target was a porous, non-flat ceramic. Four compositions were observed: 50BT-10BZT-10BS-30NN, 50BT-15BZT-15BS-20NN, 40BT-15BZT-15BS-20NN, and 45BT-17.5BZT-17.5BS-20NN.

Surprisingly, EPMA showed similar atomic percentages to what was expected from the batch composition. While the error was generally low, the average standard deviation was high. This is most likely due to the scarcity of available areas on the

pellet to take proper measurements due to their porosity. Niobium and scandium were over represented, and bismuth and titanium were under represented. Regardless, the resulting figures were relatively close to predicted atomic weight values.

Table 4.2 – EPMA results 50BT-10BZT-10BS-30NN

| **Element** | Predicted Atomic Percent | Measured Atomic Percent |
|---|---|---|
| Sodium | 6 | 6.14 |
| Scandium | 2 | 2.25 |
| Zinc | 1 | 0.88 |
| Niobium | 6 | 5.86 |
| Barium | 10 | 10.64 |
| Bismuth | 4 | 4.23 |
| Titanium | 11 | 10.33 |
| Oxygen | 60 | 59.64 |
| Error | | 1.00% |
| Standard Deviation | | 15.94% |

Table 4.3 – EPMA results 50BT-15BZT-15BS-20NN

| **Element** | Predicted Atomic Percent | Measured Atomic Percent |
|---|---|---|
| Sodium | 4 | 3.95 |
| Scandium | 3 | 3.50 |
| Zinc | 1.5 | 1.53 |
| Niobium | 4 | 3.72 |
| Barium | 10 | 10.69 |
| Bismuth | 6 | 6.14 |
| Titanium | 11.5 | 10.83 |
| Oxygen | 60 | 59.63 |
| Error | | 2.01% |
| Standard Deviation | | 17.06 % |

Table 4.4 – EPMA results 40BT-20BZT-20BS-20NN

| **Element** | Predicted Atomic Percent | Measured Atomic Percent |
|---|---|---|
| Sodium | 4 | 4.11 |
| Scandium | 4 | 4.47 |
| Zinc | 2 | 1.91 |
| Niobium | 4 | 3.82 |
| Barium | 8 | 8.72 |
| Bismuth | 8 | 7.95 |
| Titanium | 10 | 9.38 |
| Oxygen | 60 | 59.63 |
| Error | | 1.11% |
| Standard Deviation | | 16.31 % |

Table 4.5 – EPMA results 45BT-17.5BZT-17.5BS-20NN

| **Element** | Predicted Atomic Percent | Measured Atomic Percent |
|---|---|---|
| Sodium | 4 | 4.03 |
| Scandium | 3.5 | 3.90 |
| Zinc | 1.75 | 1.87 |
| Niobium | 4 | 3.99 |
| Barium | 9 | 9.84 |
| Bismuth | 7 | 6.79 |
| Titanium | 10.75 | 9.78 |
| Oxygen | 60 | 59.60 |
| Error | | 2.78% |
| Standard Deviation | | 18.63 % |

### 4.1.3 Dielectric Properties

The temperature coefficient of permittivity is calculated from permittivity data and gives a general idea of how the material's capacitance responds to temperature changes. A high temperature coefficient of permittivity signifies a strong temperature dependence. Ideally, capacitors developed in this project should possess a

temperature coefficient of permittivity that is as a low as possible. The temperature coefficients of permittivity (TCε) are shown in Table 3.2 and range from -789 to 2551 ppm °C. These results show that decreasing the tolerance factor in this system lowers the temperature coefficient of permittivity.

The relative permittivity and dielectric loss of these compositions were found experimentally and is shown in Figures 3.9 - 3.12. For all compositions, the relative permittivity increased as the temperature increased rapidly until reaching a dielectric maximum, then decreased at higher temperatures.

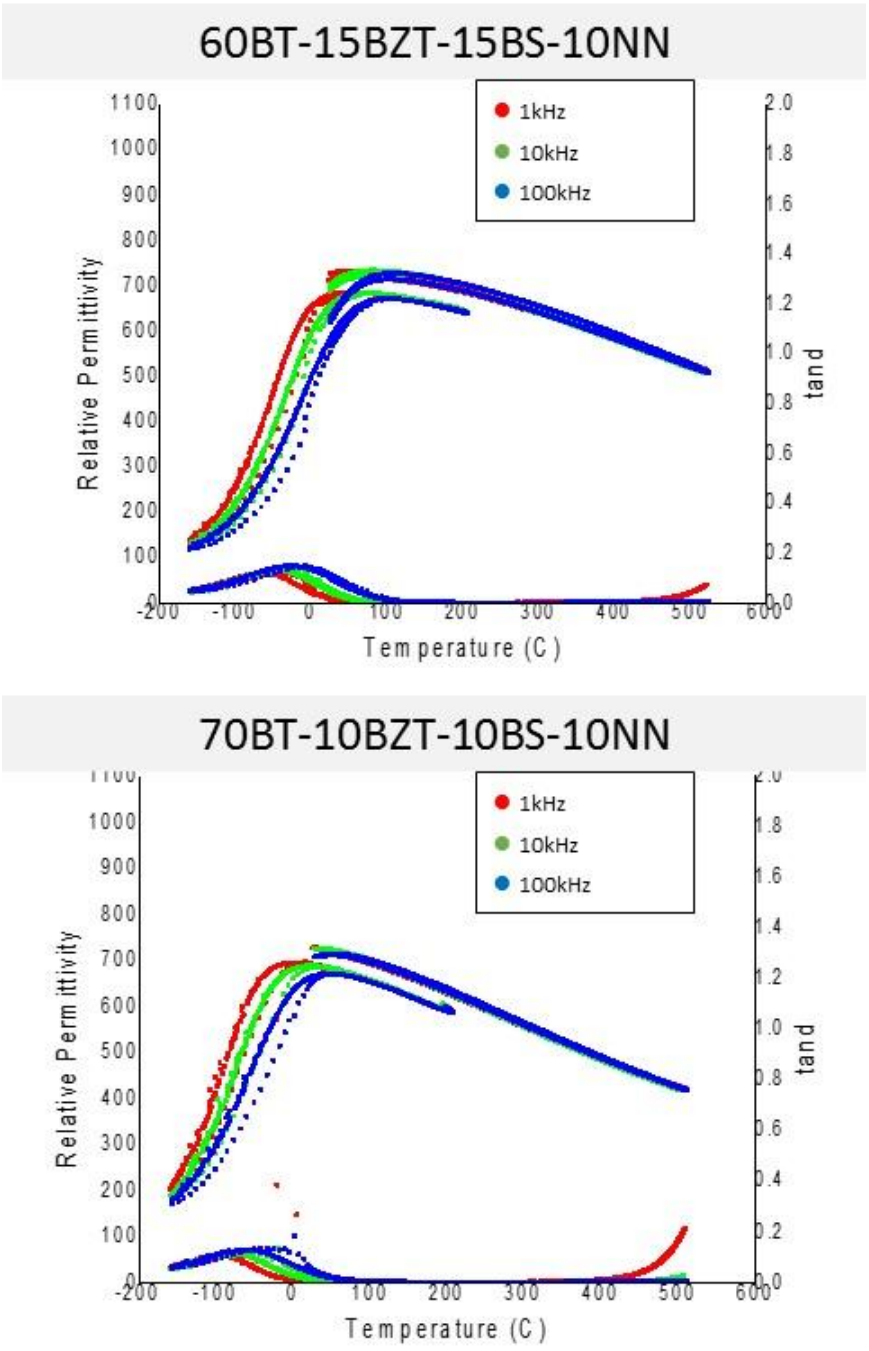


Figures 4.5 and 4.6 – Relative permittivity of 70BT-10BZT-10BS-10NN and 60BT-15BZT-15BS-10NN from -150 to 550 °C

Compositions with high-BT concentrations have overall higher relatively permittivity and low dielectric loss at the temperature ranges looked at in this study. However, due to the low concentrations of BZT-BT-NN, these compounds exhibited temperature-dependent electronic properties. Since the Curie temperature of barium titanate is 120 °C, which is not ideal, it is surprising to note that 70BT-10BZT-10BS-10NN has a greater mole fraction of BT but a lower $T_{max}$ than 60BT-15BZT-15BS-10NN. Since relaxor behavior is attributed to highly disordered B-site cations, the ferroelectric to relaxor phase transition for the 60BT composition was expected to be more diffuse, which was confirmed experimentally.

The low temperature permittivity measurements confirmed the frequency-dependent relaxor behavior at the start of the phase transition. For both compounds, the temperature of maximum permittivity approached room temperature and with low dielectric loss.

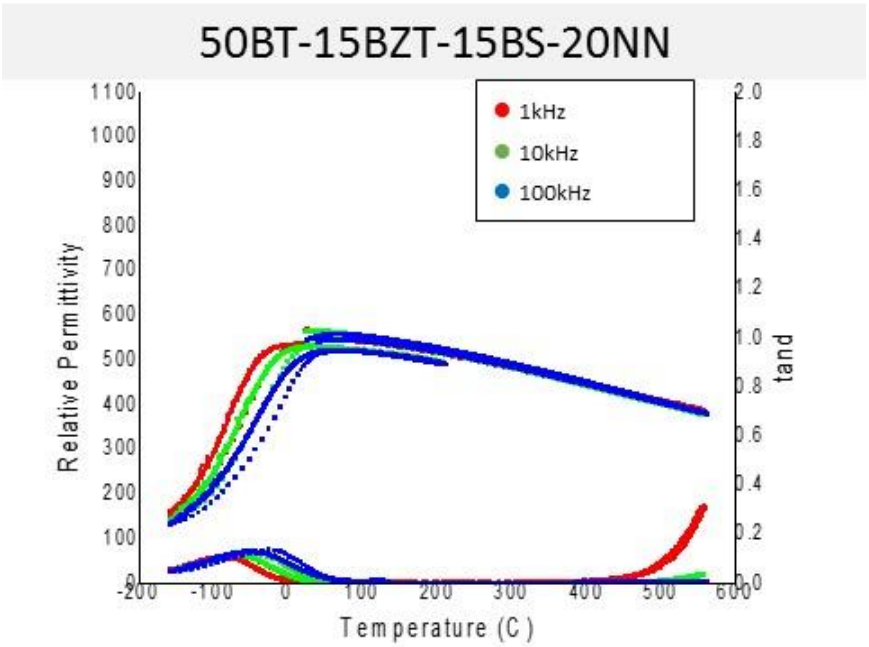


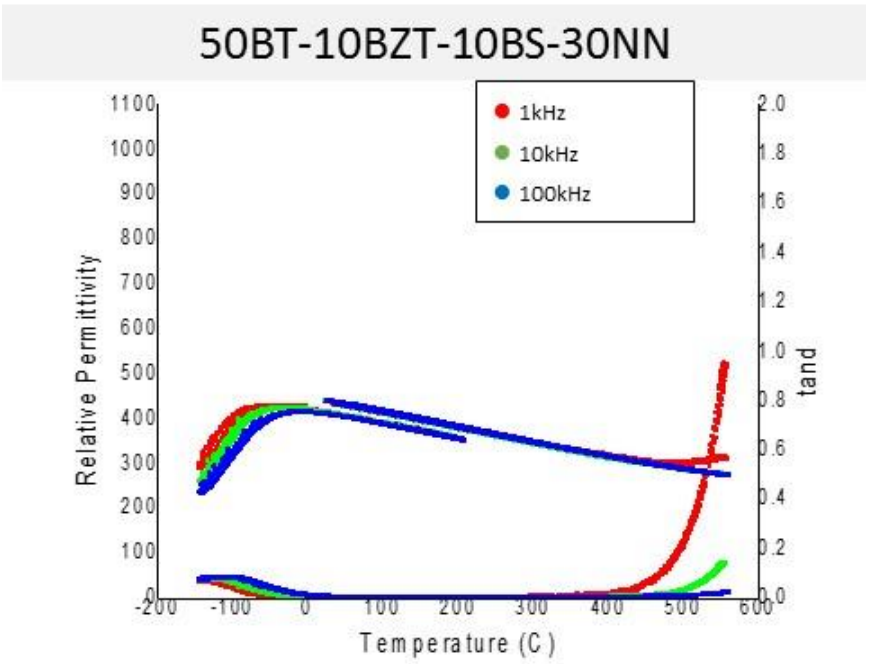


Figures 4.7 and 4.8 – Relative permittivity of 50BT-10BZT-10BS-30NN and 50BT-15BZT-15BS-20NN from -150 to 550 °C

The 50BT compositions represent ideal examples of a diffuse phase transition. At temperatures ranging from room temperature to 550 °C, the material is completely pseudo-cubic because $T_{max}$– and beginning of the phase transition – is below room temperature. Unfortunately, the relative permittivity of these materials is too low, inadequate for practical application; but by actively doping a structured barium titanate framework, the resulting compounds exhibited temperature stable dielectric properties.

For the 50BT-10BZT-10BS-30NN and 50BT-15BZT-15BS-20NN compositions, the relative permittivity values at lower temperatures demonstrate that TCε can be engineered to much lower values as compared to BT-rich compositions. The composition with the lowest $T_{max}$ is 50BT-10BZT-10BS-30NN, and it also has the highest concentration of $NaNbO_3$.

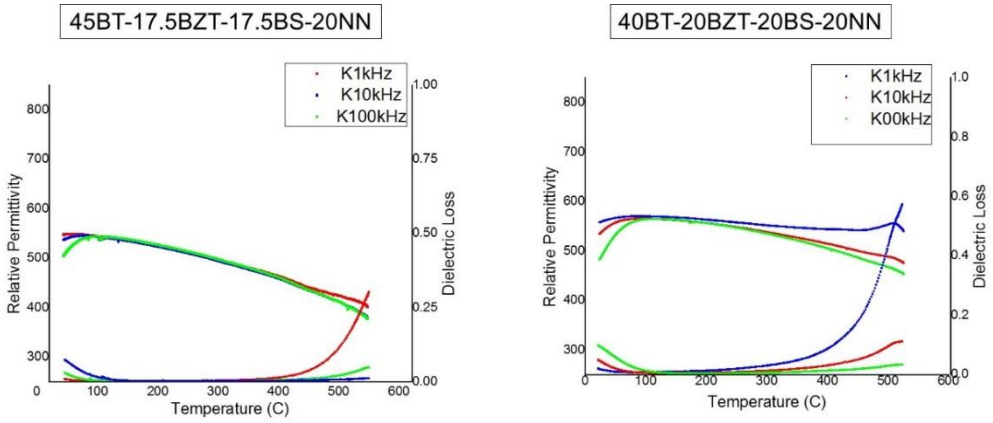


Figures 4.9 and 4.10 – Relative permittivity of 45BT-17.5BZT-17.5BS-20NN and 40BT-20BZT-120BS-20NN at high temperatures

The final two compositions in this system exhibited excellent dielectric properties. By maintaining one-to-one BZT-BS stoichiometry and keeping NN concentrations comparable to BZT-BS, the temperature coefficient of permittivity dramatically dropped to nearly zero. Therefore, the relative permittivity was nearly temperature independent. While the composition 40BT-20BZT-20BS-20NN showed increased dielectric losses at higher temperatures, this is not likely to be a problem given that this is outside the temperature ranges required for this application.

Building off previous research, the $BaTiO_3$-$Bi(Zn_{1/2}Ti_{1/2})O_3$-$BiScO_3$-$NaNbO_3$ system was investigated as a possible low temperature dielectric material. The temperature dependence of the relative permittivity was observed in compositions with decreased BT and stoichiometrically similar BZT-BS-NN. While this shift resulted in lower room temperature dielectric loss values it was also accompanied

with a lower permittivity. The $BaTiO_3$ rich compositions have a higher overall permittivity but show larger temperature coefficients of permittivity. Overall, creating an ideal material requires balancing many factors: $BaTiO_3$ allows for high permittivity; $Bi(Zn_{1/2}Ti_{1/2})O_3$-$BiScO_3$ is effective at lowering TCε; and the addition of $NaNbO_3$ was clearly effective in shifting $T_{max}$ to temperatures as low as -50°C. Since TCε describes a material's response over a range of temperatures, it can be found between any two points. For the purposes of this study, the ranges are as follows: $TC\varepsilon_{high}$ between 200 °C and 400 °C and is listed in Appendix A, $TC\varepsilon_{mid}$ between 30 °C and 300 °C, and $TC\varepsilon_{low}$ between -55 °C and 125 °C.

Table 4.6 – Ferroelectric Properties of BT-BZT-BS-NN

| **Composition** | $TC\varepsilon_{mid}$ (ppm/°C) | $TC\varepsilon_{low}$ (ppm/°C) | $T_{max}$ (°C) | ε at $T_{max}$ |
|---|---|---|---|---|
| 70BT-10BZT-10BS-10NN | -789 | 708 | 20.5 | 684.18 |
| 60BT-15BZT-15BS-10NN | -476 | 2,551 | 73.1 | 680.54 |
| 50BT-10BZT-10BS-30NN | -818 | -549 | -27.5 | 423.39 |
| 50BT-15BZT-15BS-20NN | -412 | 1,104 | 28.5 | 529.35 |
| 45BT-17.5BZT-17.5BS-20NN | -231 | - | 56.7 | 545.50 |
| 40BT-20BZT-20BS-20NN | 159 | - | 95.1 | 565.33 |

The results of this project have been presented in the paper included in Appendix A: "Relationship between tolerance factor and temperature coefficient of permittivity of temperature-stable high permittivity $BaTiO_3$ – $Bi(Me)O_3$ Compounds", published in the *Journal of Advanced Dielectrics* (Raengthon, McCue, & Cann, Relationship between tolerance factor and temperature coefficient of

permittivity of temperature-stable high permittivity BaTiO3-Bi(Me)O3 Compounds, 2015). Along with the $BaTiO_3$-$Bi(Zn_{1/2}Ti_{1/2})O_3$, $BaTiO_3$-$Bi(Zn_{1/2}Ti_{1/2})O_3$-$BiInO_3$, and $BaTiO_3$-$Bi(Zn_{1/2}Ti_{1/2})O_3$-$BiScO_3$ systems, a trend was observed linking microscopic crystal chemical properties (the tolerance factor) with the electronic properties.

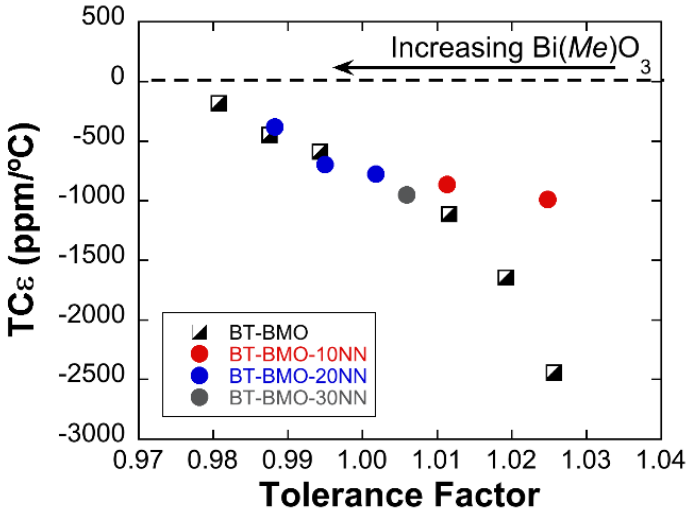


Figure 4.11 – Tolerance factor as it relates to the TCε of BT-B(M) compounds

As the tolerance factor of a solid solution relaxor perovskite decreased, the temperature coefficient of permittivity approached values close to zero. This suggests that TCε can be engineered and controlled by designing and tuning compositions. This general relationship between TCε and the tolerance factor can be used as a guide to design new high permittivity compounds with temperature-stable permittivity characteristics for practical capacitor application.

## 4.2 Temperature Stable Dielectrics Based on Pb-based Relaxors

Creating a dielectric material with ideal temperature-stable properties is a challenge that requires combining a variety of relaxor compounds into one solid solution. Previously, the lead-free system $BaTiO_3$-$Bi(Zn_{1/2}Ti_{1/2})O_3$-$BiScO_3$-$NaNbO_3$ (BT-BZT-BS-NN) was investigated with mixed results. Unfortunately, while these compounds were lead-free and thus minimizing pollution and harmful toxins, the dielectric properties fell short of the goal of this project. A new family of materials was developed to meet the goals with lead-based compounds. The introduced lead materials investigated typically have higher permittivity values and lower $T_{max}$.

Previous research on many ferroelectric relaxor systems containing $BaTiO_3$, $Bi(Zn_{1/2}Ti_{1/2})O_3$, $Pb(Ni_{1/3}Nb_{2/3})O_3$ and $Pb(Mg_{1/3}Nb_{2/3})O_3$ (BT-BZT-PNN/PMN) have observed their electronic and mechanical properties. Going back to the 1950s, polycrystalline PNN and PMN were some of the first relaxors ever discovered and have been thoroughly researched. The ferroelectric to relaxor phase transition for polycrystalline PNN exists at -120 °C (Alberta & Bhalla, Low-Temperature Properties of Lead Nickel-Niobate Ceramics, 2002). For PMN, the same transition happens at a higher temperature of - 48°C (Fu, Taniguchi, Itoh, & Mori, 2012).

Both PNN and PMN possess the perovskite structure with a ferroelectric to relaxor phase transitions ideal for this project. In building off of the last study, the goal is to substitute $BiScO_3$ and $NaNbO_3$ with classical Pb-based relaxor materials to create a solid solution that can be used as a low temperature dielectric capacitor.

### 4.2.1 Processing

Just like before, the first step to create these solid solutions is to find an ideal synthesis route. Unfortunately, the creation of a PMN perovskite via the solid-state synthesis reaction has problems with the naturally occurrence of pyrochlore-type phase impurities due to the volatile nature of PbO, the low dispersion of MgO, and the large difference bond strengths between Pb-Nb and Pb-Mg (Wongmaneerung, Sarakonsri, Yimnirun, & Ananta, 2006). It has been shown that using a two-step process can produce phase pure PMN and the synthesis route tremendously reduces the concentration of impurities. This method is called the B-site precursor approach, or the columbite synthesis route (Swartz & Shrout, 1982). In this method, an intermediate step is used to create pure columbite $MgNb_2O_6$ which is then combined with lead oxide, PbO. There are two alternatives that were not investigated in this study. One approach is to create columbite $MgNb_2O_6$ but add in excess PbO and nitric acid to remove any excess MgO in the system. Another option is to first synthesize corundum $Mg_4Nb_2O_9$ and use it as a precursor, but there are few literature reports on the process. For the purposes of this investigation, the columbite method was chosen as the ideal synthesis route.

Just like PMN, PNN also has processing challenges for similar reasons. These perovskites are analogous due to the fact that the $Ni^{2+}$ and $Mg^{2+}$ ion are similarly sized (70 pm and 72 pm, respectively). In fact, the same columbite precursor method

also works with PNN by first creating $NiNb_2O_6$ and mixing with PbO (Alberta & Bhalla, Low-temperature properties of lead nickel-niobate ceramics, 2002).

The BT-BZT-PNN and BT-BZT-PMN systems both contain a mixture of classical relaxors that can be combined to create a solid solution with ideal electronic properties. The goal is to create a composition with a diffuse ferroelectric to relaxor phase transition that starts well below room temperature while maintaining an adequate permittivity for high voltage capacitor applications.

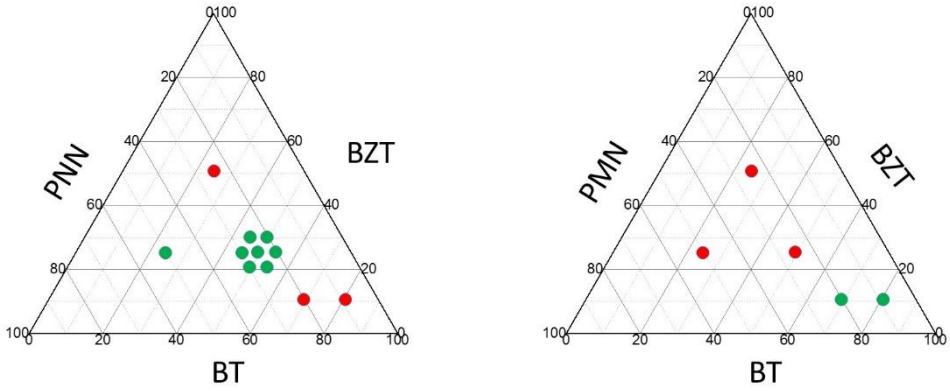


Figure 4.12 and 4.12 – Phase diagrams for the BT-BZT-PNN and BT-BZT-PMN systems; green is single phase material; red is mixed phase

## 4.2.2 Physical Characterization

Both BT-BZT-PNN and BT-BZT-PMN have not been previously investigated, so once a synthesis procedure is finalized, the next step is to establish the stable perovskite phase field on the ternary phase diagram. To understand the system, three solid solutions were initially made for *x*BT-*x*BZT-*x*PNN and *x*BT-*x*BZT-*x*PMN

where $x$ = 25 or 50. Results were not successful: single phase perovskite was not obtained in any of the PMN-based compositions. In the previous study, compounds of higher BT concentration generally were of single phase, so that was attempted next – for PMN this was successful in creating a single phase perovskite composition. However, after the creation of ceramic pellets, dielectric measurements showed undesirable electronic properties.

X-ray diffraction (XRD) data on the BT-BZT-PNN single phase material is shown in Figure 4.6. At room temperature, 50BT-25BZT-25PNN is cubic due to the singlet (200) peak, which was also confirmed as $T_{max}$ was at 46.7 °C. All compositions of similar stoichiometry to 50BT-25BZT-25PNN were found to be single phase.

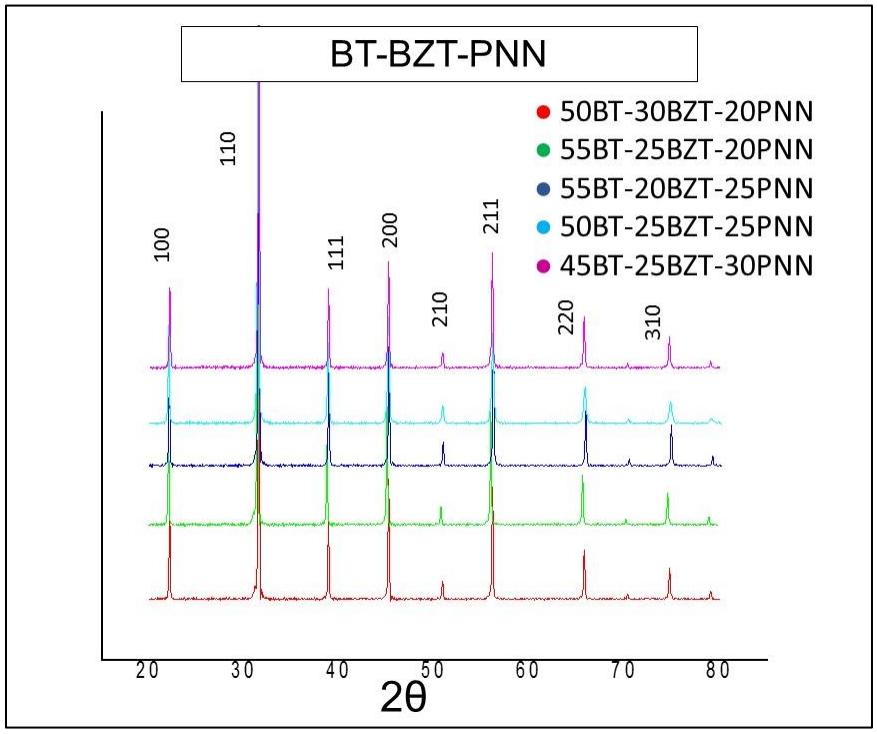


Figure 4.14 – X-ray diffraction data of the BT-BZT-PNN system

After single phase BT-BZT-PNN with promising dielectric properties was found, similar compositions were investigated that are shown in Figure 4.1. Due to the difficulties of processing these kinds of materials, one outlier exists: 49BT-

29BZT-22PNN. There was a problem during the weighing of precursors that could not be remedied, but the compound was sintered and tested anyways. Permittivity data in Figure 4.7 and it is clear that temperature strongly effects dielectric properties due to high TCε.

Table 4.7 – Physical properties of BT-BZT-PNN

| **Composition** | **Lattice Parameter (Å)** | **Theoretical Density(g/cm$^3$)** | **Measured Density (g/cm$^3$)** | **Tolerance Factor** |
|---|---|---|---|---|
| 55BT-20BZT-25PNN | 4.0167 | 7.144 | 5.93 | 1.014 |
| 55BT-25BZT-20PNN | 4.0153 | 7.028 | 6.14 | 1.013 |
| 50BT-30BZT-20PNN | 4.0157 | 7.056 | 5.64 | 1.007 |
| 50BT-25BZT-25PNN | 4.0176 | 7.184 | 5.96 | 1.008 |
| 45BT-25BZT-30PNN | 4.0187 | 7.275 | - | 1.004 |
| 49BT-29BZT-22PNN | - | - | - | 1.007 |

## 4.2.3 Dielectric Characterization

While maintaining a high relative permittivity with a low $T_{max}$, 80BT-10BZT-10PMN and 70BT-10BZT-20PMN exhibit incredibly large temperature coefficients of permittivity. Even after obtaining single phase perovskite, the system itself is suboptimal for the purposes of this project. The BT-BZT-PMN and BT-BZT-PNN phase diagrams are shown in Figures 4.1 and 4.2.

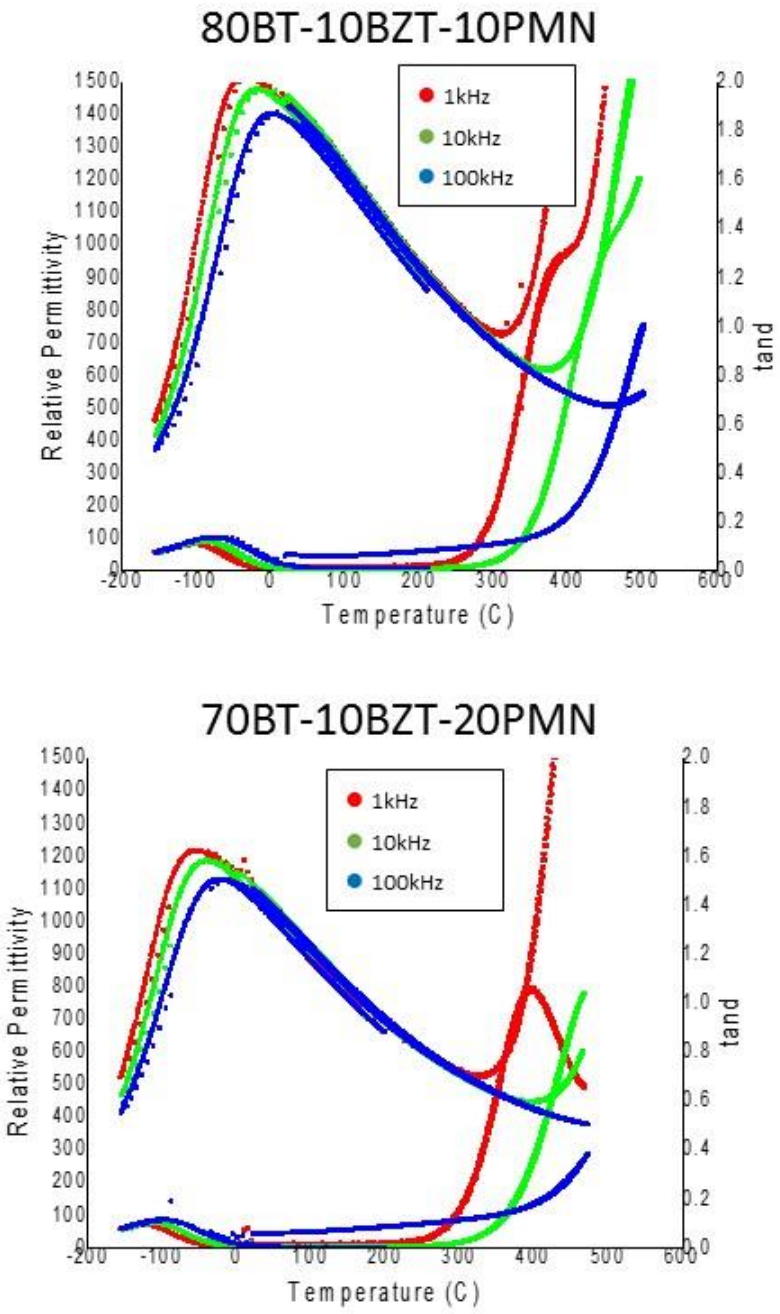


Figure 4.15 and 4.16 – High temperature permittivity of 80BT-10BZT-10PMN and 70BT-10BZT-20PMN from -150 to 550 °C

There were more promising results with the BT-BZT-PNN system as a possible linear dielectric. Permittivity measurements of the single phase initial compositions showed promising relaxor behavior for 50BT-25BZT-25PNN. Although $T_{max}$ is near RT, its electronic properties are generally temperature stable up to 300 °C. The 25BT-25BZT-50PNN solid solution exhibited similar deficiencies as the PMN based system: the temperature coefficient of permittivity was too large and further research on similar stoichiometric compositions was not pursued.

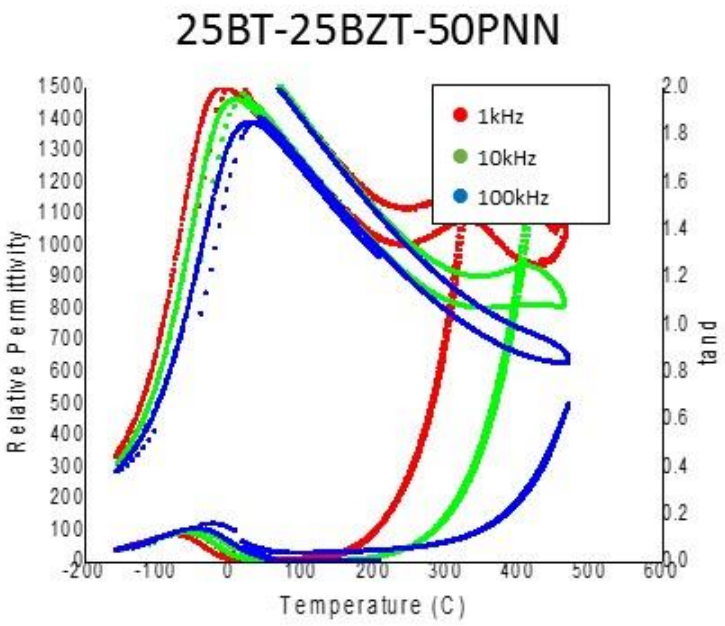


Figure 4.17 – Relative permittivity of 25BT-25BZT-50PNN from -150 to 550 °C

There was greater success with BT-BZT-PNN as a possible linear dielectric. Permittivity measurements of the initial single phase compositions showed promising relaxor behavior for 50BT-25BZT-25PNN. Although T was above RT, its electronic properties are generally temperature stable up to 300 °C. The 25BT-25BZT-50PNN solid solution exhibited similar problems as the PMN based system: the temperature coefficient of permittivity was too large and further research on similar stoichiometric compositions was not pursued. Compositions of similar stoichiometry to 50BT-25BZT-25PNN were investigated in this study.

The temperature coefficients of permittivity (TCε) are calculated directly from dielectric data and are shown in Table 4.2. There was a wide range of TCε values for varying temperature ranges due to the fact that the BT-BZT-PNN compositions presented in this study have wide ranging ferroelectric-to-relaxor phase transition between -13.4 and 77.2 °C. Unlike the previous system, no correlation was found that linked tolerance factor and TCε.

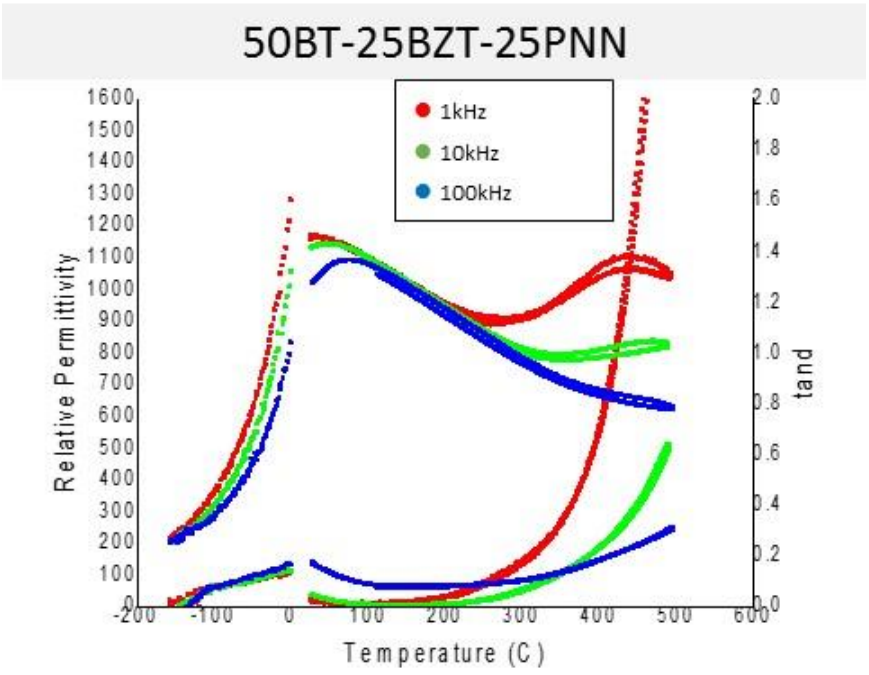


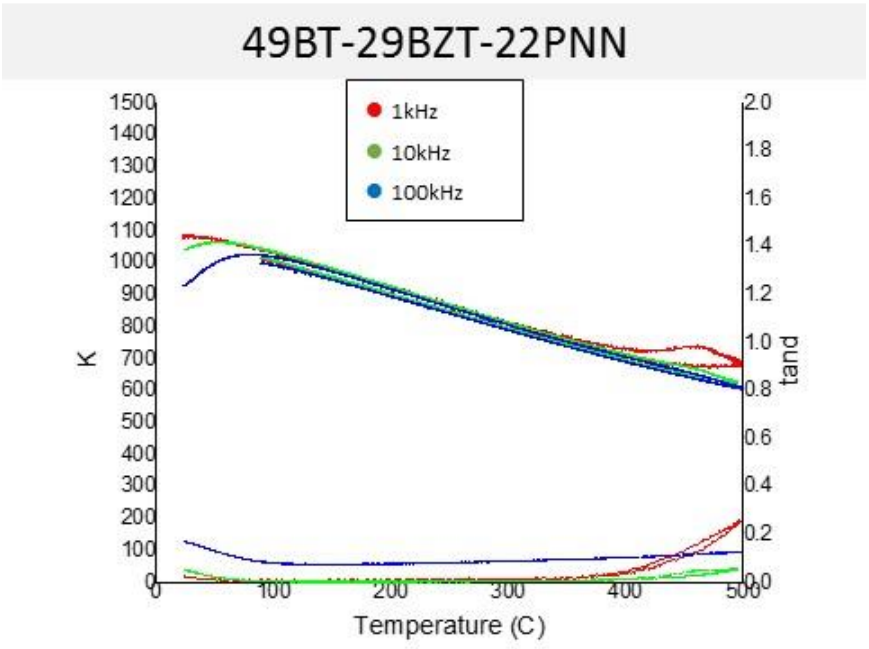


Figures 4.18 and 4.19 – Relative permittivity of 50BT-25BZT-25PNN and 49BT-29BZT-22PNN from -150 to 550 °C

The majority of compositions of the BT-BZT-PNN system show relatively high permittivity compared to similar relaxors. Unfortunately, temperature stability was not always maintained as often these materials exhibit high dielectric variance.

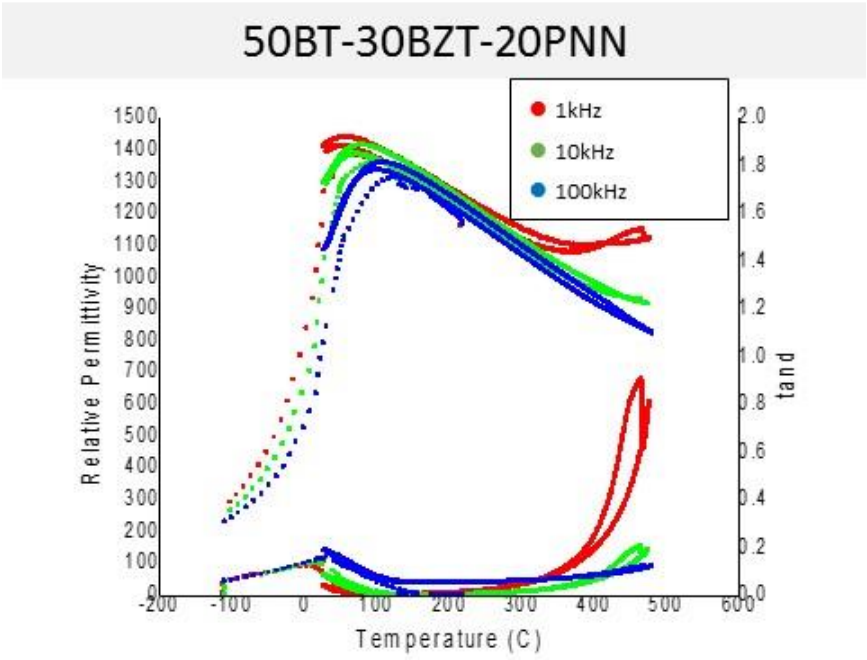


Figure 4.20 – Relative permittivity of 50BT-30BZT-20PNN from -150 to 550 °C

Some compositions did not produce high quality data with measurements at low temperatures. In particular, 1kHz data for 55BT-20BZT-25PNN was unintelligible and noisy. Curiously, all low temperature permittivity for 45BT-25BZT-30PNN was incredibly lossy and the data suggests the sample was conductive below 10 °C, although further research is needed.

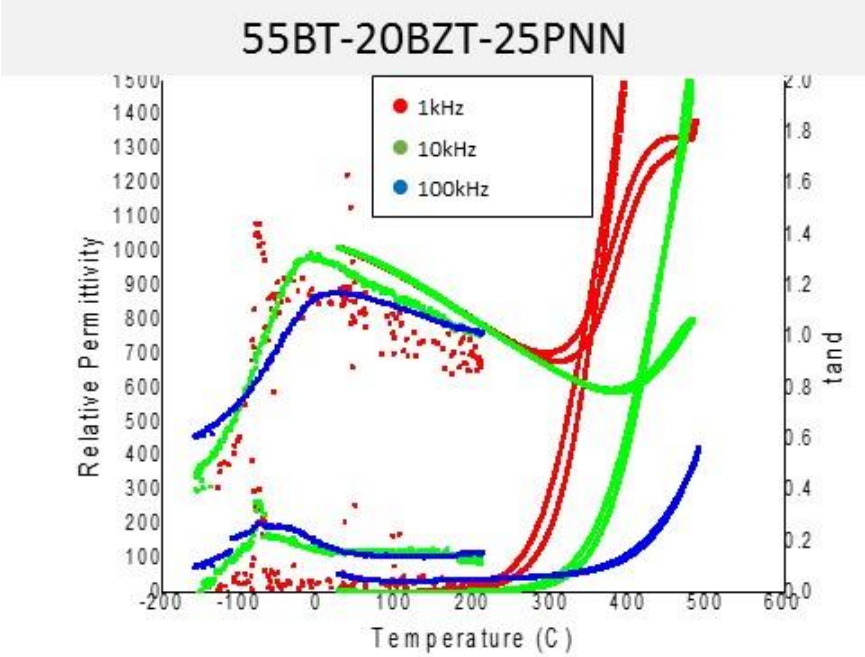


Figure 4.21 - Relative permittivity of 55BT-20BZT-25PNN from -150 to 550 °C

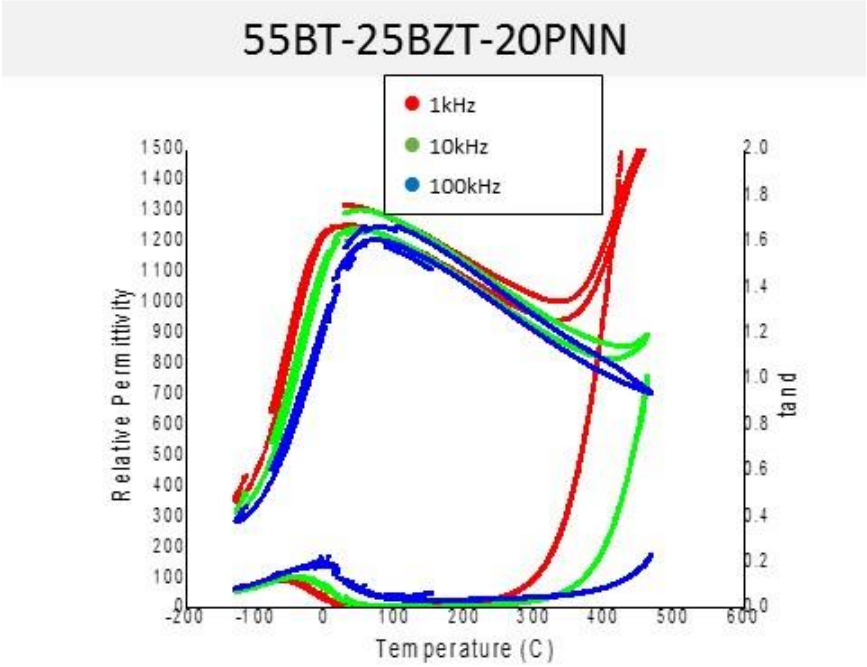


Figure 4.22 – Relative permittivity of 55BT-25BZT-20PNN from -150 to 550 °C

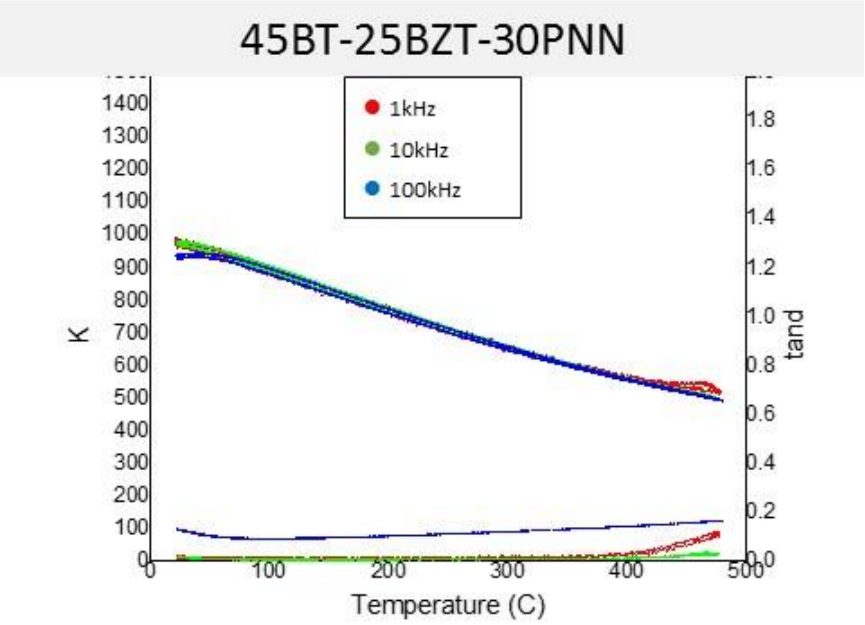


Figure 4.23 – High temperature permittivity of 45BT-25BZT-30PNN

The BT-BZT-PMN system was investigated and produced poor results in reference to the goals of this study. As a possible complex perovskite dielectric, BT-BZT-PNN exhibits interesting ferroelectric properties that could make it suitable for capacitor applcation. By far the best composition presented in the BT-BZT-PNN system is 55BT-20BZT-25PNN. It has great dielectric properties suitable for a wide range off temperatures. With a $T_{max}$ below 0 °C, the highest maximum relative permittivity, and an incredibly small TCε between -55 - 125 °C , it fullfills the goals of this study. As a reminder, TCε ranges are as follows: $TC\varepsilon_{high}$ between 200 °C and 400 °C, $TC\varepsilon_{mid}$ between 30 °C and 300 °C, and $TC\varepsilon_{low}$ between -55 °C and 125 °C.

Table 4.8 – Ferroelectric properties of BT-BZT-PNN

| **Composition** | $TC\varepsilon_{mid}$ (ppm/ºC) | $TC\varepsilon_{low}$ (ppm/ºC) | $T_{max}$ (ºC) | ε at $T_{max}$ |
|---|---|---|---|---|
| 55BT-20BZT-25PNN | -1293 | 44 | -13.4 | 1004.49 |
| 55BT-25BZT-20PNN | -748 | 2521 | 35.1 | 1292.70 |
| 50BT-30BZT-20PNN | -1014 | 2685 | 46.7 | 1136.85 |
| 50BT-25BZT-25PNN | -173 | 3989 | 77.2 | 1409.33 |
| 45BT-25BZT-30PNN | -1317 | - | 22.6 | 976.70 |
| 49BT-29BZT-22PNN | -717 | - | 55.2 | 1059.95 |

# Chapter 5 – Discussion

High performance dielectric materials are needed for high power SiC- or GaN-based electronics which combine the best features of high energy density, low dielectric loss and high reliability and for advanced high-speed and high-voltage energy storage where temperature plays an important role in material properties. An ideal capacitor for these systems has temperature-stable permittivity characteristics, a maximum permittivity near or below 0 °C, and sufficiently high permittivity to have practical application. This work involves the synthesis, processing, characterization, testing, and evaluating of the compositions $BaTiO_3$-$Bi(Zn_{1/2}Ti_{1/2})O_3$-$BiScO_3$-$NaNbO_3$, $BaTiO_3$- $Bi(Zn_{1/2}Ti_{1/2})O_3$-$Pb(Mg_{1/3}Nb_{2/3})O_3$, and $BaTiO_3$- $Bi(Zn_{1/2}Ti_{1/2})O_3$-$Pb(Ni_{1/3}Nb_{2/3})O_3$, all of which were investigated as possible linear dielectric capacitor materials. These materials have excellent dielectric properties due to a relaxor dielectric mechanism which is derived from B-site cation disorder. Typical relaxor diffuse phase transition behavior allows for large temperature ranges of similar electronic properties. These systems have been shown to have relatively easy synthesis routes, creating single-phase solid solutions. More investigation is necessary to find ideal dielectric properties.

The Pb-free system $BaTiO_3$-$Bi(Zn_{1/2}Ti_{1/2})O_3$-$BiScO_3$-$NaNbO_3$ has shown promising linear dielectric properties when BZT-BS-NN are at or near stoichiometric amounts. However, lower amounts of BT threaten to undermine single phase stability. The electronic properties of this quaternary system, which was investigated due to

promising research on its individual parts, has been shown to relate directly to physical properties. The tolerance factor of BT-BZT-BS-NN is directly correlated to its temperature coefficient of permittivity. As the tolerance factor decreases, the system's dielectric response becomes more temperature independent between -55 °C to 175 °C. The compositions with the lowest temperature coefficient of permittivity and tolerance factor have the general makeup *2x*BT-*y*BZT-yBS-*x*NN where x and y are near 20 atomic percent and have similar stoichiometry. Single phase material was unable to be synthesized when the atomic percent of barium titanate was below 40 percent. The possible capacitors that could be created with proper government classification are: 50BT-10BZT-10BS-30NN (X7R, Y5V), 60BT-15BZT-15BS-10NN (Y5V), 50BT-15BZT-15BS-20NN (Y5V), 45BT-17.5BZT-17.5BS-20NN (Y5V), and 40BT-20BZT-20BS-20NN (Y5V). Typically, these compositions also exhibited temperatures of maximum permittivity below 0 °C, which is one of the major goals of this project.

The $BaTiO_3$- $Bi(Zn_{1/2}Ti_{1/2})O_3$-$Pb(Mg_{1/3}Nb_{2/3})O_3$ system was found to be non-viable as potential linear dielectric. Single phase material was only possible at high stoichiometric amounts of barium titanate but with non-ideal electronic properties. Further research into BT-BZT-PMN was not pursued once it became clear there would be no application of the materials.

The best material for use as a linear dielectric at room temperature was the $BaTiO_3$- $Bi(Zn_{1/2}Ti_{1/2})O_3$-$Pb(Ni_{1/3}Nb_{2/3})O_3$ system due to its low temperature

coefficient of permittivity and adequate capacitance. In particular, the 55BT-20BZT-25PNN has great dielectric properties suitable for a wide range off temperatures. With a $T_{max}$ at below 0 °C, a maximum relative permittivity near 1000, and an incredibly small TCε between -55 - 125 °C , it is an ideal capacitor that fullfills the goals of this study. Compared to BT-BZT-BS-NN, BT-BZT-PNN compounds have almost double the capacitance while maintaining a similar temperature dependence. Unfortunately, for some compositions, the temperatures of maximum permittivity are too high, and these systems would not meet the specifications between -55°C to 125°C. The possible capacitors that could be created with proper government classification are: 55BT-20BZT-25PNN (X7R, Y5V), 55BT-25BZT-20PNN (X9R), and 50BT-25BZT-25PNN (X9R). Further work is needed to shift the temperature of the diffuse phase transition for these compounds to temperatures below 0°C.

# Chapter 6 – Future Work

The goal of this project has been to create temperature stable dielectrics for SiC- or GaN-based electronics and advanced high-speed and high-voltage energy storage. The compositions studied have provided a framework for future work which would involve compositional modifications aimed at increasing the relative permittivity which would allow device miniaturization as well characterization of the dielectric properties at high electric fields (E > 100 kV/cm).

More research will be required to determine the limits of the BT-BZT-BS-NN quaternary system. An interesting suggestion would be to look at compositions between or near 45BT-17.5BZT-17.5BS-20NN and 40BT-20BZT-20BS-20NN. Both compositions provided low temperature coefficients of permittivity at ambient temperatures. Also, non-stoichiometric compositions within the BZT-BS system have not yet been investigated in this quaternary system, so future research could elucidate the differences between BZT and BS as relaxor ferroelectrics in solid solutions. For a low temperature linear dielectric, the BT-BZT-BS-NN shows the most promise even with its generally low capacitance. However, the capacitance can be artificially increased by creating a larger device or increasing the number of layers in a multilayer capacitor, neither of these techniques would affect the promising dielectric properties of the system.

Due to the failure of $BaTiO_3$- $Bi(Zn_{1/2}Ti_{1/2})O_3$-$Pb(Mg_{1/3}Nb_{2/3})O_3$, this composition should not be investigated any further due to processing problems.

Creating a single phase perovskite material was nearly impossible, and any successful synthesis was met by inferior electronic properties. However, more research could be necessary to entirely rule out the system. Only five compositions were synthesized and tested: there is the possibility of single phase material in other regions of the phase diagram, but for the purpose of this thesis they were not investigated.

The most promising composition and the best candidate for future work is the $BaTiO_3$- $Bi(Zn_{1/2}Ti_{1/2})O_3$-$Pb(Ni_{1/3}Nb_{2/3})O_3$ system due to its low temperature coefficient of permittivity and average capacitance. Utilizing the tedious columbite method during synthesis removes possible pyrochlore impurities and allows for a stable perovskite solid solution. The BT-BZT-PNN system shows promising dielectric properties and could be further investigated at different compositions than those presented in this thesis. However, the generally low maximum temperatures of permittivity are not ideal for a low temperature dielectric.

The biggest obstacle to create stable dielectrics with temperature independent electric properties is the relatively low permittivity compared to industry standard capacitors. To increase the overall permittivity, BT could be replaced with a Pb-based compound while ensuring that the other compounds are not Pb-based to ensure long range disorder, a requirement for relaxor ferroelectrics. For example, the most commonly used piezoelectric is $Pb(Zn_{0.48}Ti_{0.52})O_3$ (PZT). Using PZT instead of BT as a framework while adding BZT and NN could create linear dielectrics with naturally higher permittivities than BT-based compositions.  Another example of further

research could be to replace BT with $SrTiO_3$ (ST), a classic paraelectric material. Strontium titanate has a cubic structure and a tolerance factor equal to unity. Doping with a ST-based system could lower the lattice tolerance factor, which has been shown to decrease the temperature coefficient of permittivity.

# Bibliography

Alberta, E., & Bhalla, A. (2002). Low-temperature properties of lead nickel-niobate ceramics. *Materials Letters, 54*, 47-54.

Alberta, E., & Bhalla, A. (2002). Low-temperature Properties of Lead Nickel-Niobate Ceramics. *Materials Letters*, 47-54.

Alberta, E., & Bhalla, A. (2002). Low-Temperature Properties of Lead Nickel-Niobate Ceramics. *Materials Letters, 54*, 47-54.

Ansell, T., Nikkel, J., Cann, D., & Sehirioglu, A. (2012). High Temperature Piezoelectric Ceramics Based on xPbTiO3-(1-x)Bi(Sc1/2Me1/4Ti1/4)O3 (Me = An, Mg) Ternary Perovskites. *Japanese Journal of Applied Physics, 51*, 101802.

Bengisu, M. (n.d.). *Engineering Ceramics.* 2001: Springer .

Bokov, V., & Myl'nikova, I. (1959). *Kristallografia, 4*, 433.

Bouzid, A., Bourim, E., Gabbay, M., & Fantozzi, G. (2005). PZT Phase Diagram Determinaton by Measurement of Elastic Moduli. *Journal of the European Ceramic Society, 25*, 3213-3221.

Breitkopf, C. (2012). Impedance Spectroscopyu. *Lecture Series at Fritz-Haber-Institute Berlin*, 17.

Caspari, M. a. (1950). The Electromechanical Behavior of BaTiO3 Single-domain Crystals. *Physical Review, 80*(6), 1082-1089.

Chakhmouradian, A., & Woodward, P. (2014). Celebrating 175 years of perovskite research: a tribute to Roger H. Mitchell. *Physics and Chemistry of Minerals, 41*, 387-391.

Eckert, M. (2012). Max von Laue and the Discovery of X-ray Diffraction in 1912. *Annalen der Physik, 5*, 82-85.

Evans, J. (n.d.). *Ferrodevices.* Retrieved from http://www.ferrodevices.com/1/297/files/chapter4-theoryofferroelectriccapacitors.pdf

Forsbergh, P. (1949, October). Domain Structures and Phase Transitions in Barium Titanate. *Physical Review Letters, 76*, 1187.

Fu, D., Taniguchi, H., Itoh, M., & Mori, S. (2012). Pb(Mg1/3Nb2/3)O3 (PMN) Relaxor: Dipole Glass or Nano-Domain Ferroelectric ? *Advances in Ferroelectrics*, 51-67.

Hong, C., Kim, H., Choi, B., Han, H., Son, J., Ahn, C., & Jo, W. (2016, March). Lead-free piezoceramics - Where to moveon? *Journal of Materiomics, 2*(1), 1-24.

Keithly, J. (1999). *The Story of Electrical and Magnetic Measurements: From 500 BC to the 1940s.* Wiley IEEE Press.

Koerver, H. (2012). *German Submarine Warfare 1914-1918 in the Eyes of British Intelligence.* Berlin: LIS Reinisch.

Kolkin, A. P., & Goltsev, A. (2008). Piezoelectricty and Crystal Symmetry. In A. Safari, & E. Akdogan, *Piezoelectric and Acoustic Materials for Transducer Applications* (pp. 17-19). Springer US.

Lee, S., Randall, C., & Liu, Z. (2009, January). Factors Limiting Equilibium in Fabricating Simple Ferroelectric Oxide BaTiO3. *Journal of the American Ceramic Society, 92*, 222-228.

Macutkevic, J., Banys, J., Bussman-Holder, A., & Bishop, A. (2011). Origin of Polar Nanoregions in Relaxor Ferroelectrics: Nonlinearity, Discrete Breather Formation, and Charge Transfer. *Physical Review B, 83*, 184301.

Mayergoyz, I. a. (2005). *The Science of Hysteresis* (Vol. 3). Cambridge: Academic Press.

Merz, W. (1949). The Electric and Optical Behavior of BaTiO3 Single-Domain Crystals. *American Phyisical Society, 76*, 1221.

Merz, W. (1954). Domain Formation and Domain Wall Motions in Ferroelectric BaTiO3 Single Crystals. *Physical Review, 95*(3), 690-698.

*Multilayer Ceramic Capacitors/Axial & Radial Leaded.* (n.d.). Retrieved from www.kemet.com: http://www.kemet.com//Lists/ProductCatalog/Attachments/52/F3101_GoldMax.pdf

Raengthon, N., & Cann, D. (2011). Dielectric Relaxation in BaTiO3-Bi(Zn1/2Ti1/2)O3 Ceramics. *Journal of the American Ceramic Society, 95*(5), 1604-1612.

Raengthon, N., Brown-Shaklee, H., Brennecka, G., & Cann, D. (2013). Dielectric Properties of BaTiO3-Bi(Zn1/2Ti1/2)O3-NaNbO3 Solid Solutions. *Journal of Material Science, 48*, 2245-2250.

Raengthon, N., DeRose, V., Brennecka, G., & Cann, D. (2012). Defect Mechanisms in High Resistivity BaTiO3-Bi(Zn1/2Ti1/2)O3 Ceramics. *Applied Physics Letters, 101*, 112904.

Raengthon, N., McCue, C., & Cann, D. (2015). Relationship between tolerance factor and temperature coefficient of permittivity of temperature-stable high permittivity BaTiO3-Bi(Me)O3 Compounds. *Journal of Advanced Dielectrics*.

Raengthon, N., Sebastian, T., Cumming, D., Reaney, I., & Cann, D. (2012). BaTiO3-Bi(Zn1/2Ti1/2)O3-BiScO3 Ceramics of High-Temperature Capacitor Applications. *Journal of the American Ceramic Society, 95*(11), 3554-3561.

Randall, C. a. (2004). *History of the First Ferroelectric Oxide, BaTiO3.* Retrieved from ceramics.org.

Rase, D., & Roy, R. (1955, March). Phase Equilibria in the System BaO-TiO2. *Journal of the American Ceramic Society, 38*(3), 102-113.

Remeika, J. (1954). A Method for Growing Barium Titanate Single Crystals. *Journal of the American Ceramic Society, 76*, 940.

Shannon, R. (1976). Revised Effective Ionic Radii and Systematic Studies of Interatomic Distances in Halides and Chalcogenides. *Acta Cryst.*, 751-767.

Smith, M., Page, K., Siegrist, T., Redmond, P., Walter, E., Seshadri, R., . . . Steigerwald, M. (2008). Crystal Structure and the Paraelectric-to-Ferroelectric Phase Transition of Nanoscale BaTiO3. *Journal of the American Chemical Society, 130*, 6955-6955.

Smith, R. T. (1967). Elastic Piezoelectric, and Dielectric Properties of Lithium Tantalate. *Applied Physics Letters, 11*, 146-148.

Smolenski, A., & Agronovskaya, A. (1958). Dielectric Polarization and Losses of Some Complex Compounds. *Soviet Physics: Technical Physics, 3*(7), 1380-1382.

Swartz, S., & Shrout, T. (1982). *Mat. Res. Bull., 17*, 1245-1250.

Viehland, D., Jang, S., Cross, L., & Wuttig, M. (1990). Freezzing of the Polarization Fluctuations in Lead Magnesium Niobate Relaxors. *Journal of Applied Physics, 68*, 2916.

Wada, S., Kakemoto, H., & Tsurumi, T. (2004). Enhanced Piezoelectric Properties of Piezoelectric Single Crystals by Domain Engineering. *Materials Transactions, 45*(2), 178-187.

Wongmaneerung, R., Sarakonsir, T., Yimnirun, R., & Ananta, S. (2006). Effects of Magnesium Niobate Precursor and Calcination Condition on Phase Formation and Morphology of Lead Magnesium Niobate Powders. *Materials Science and Engineering*, 292-299.

Wongmaneerung, R., Sarakonsri, T., Yimnirun, R., & Ananta, S. (2006). Effects of magnesium niobate precursor and calcination conditions on phase formation and morphology of lead magnesium niobate powders. *Materials Science and Engineering B*, 292-299.

Yamada, T., Niizeki, N., & Toyoda, H. (1967). Piezoelectric and Elastic Properties of Lithium Niobate Single Crystals. *Japanese Journal of Applied Physics, 6*(2), 151-.

Zahn, M. (1988, October). The Contributions of Arthur Robert von Hippel to Electrical Insulation Research. *IEEE Transactions on Electrical Insulation, 23*(5), 791-800.

Zimmerman, D. (2002, January). Paul Langevin and the Discovery of Active Sonar or Asdic. *The Northern Marine/Le marin du nord, 12*(1), 39-52.

# APPENDIX A

## Relationship between tolerance factor and temperature coefficient of permittivity of temperature-stable high permittivity $BaTiO_3$ – Bi($Me$)$O_3$ Compounds

**JOURNAL OF ADVANCED DIELECTRICS**

**Vol. 6, No. 1 (March 2016)**

Natthaphon Raengthon[†,‡,*] , Connor McCue[‡] and David P. Cann[‡]

[†]*Department of Materials Science, Faculty of Science, Chulalongkorn University, Pathumwan, Bangkok, 10330, Thailand*

[‡]*Materials Science, School of Mechanical, Industrial, and Manufacturing Engineering, Oregon State University, Corvallis, Oregon 97331, USA*

[*]Natthaphon.R@chula.ac.th

Received 18 November 2015; Revised 7 December 2015; Accepted 8 December 2015; Published 16 February 2016

**Abstract**

The temperature coefficient of permittivity of $BaTiO_3$ – Bi($Me$)$O_3$ solid solutions were investigated. It was determined that as the tolerance factor was decreased with the addition of Bi($Me$)$O_3$, the temperature coefficient of permittivity ($TC\varepsilon$) shifted from large negative values to $TC\varepsilon$ values approaching zero. It is proposed that the

different bonding nature of the dopant cation affects the magnitude and temperature stability of the permittivity. This study suggests that the relationship between tolerance factor and temperature coefficient of permittivity can be used as a guide to design new dielectric compounds exhibiting temperature-stable high permittivity characteristics, which is similar to past research on perovskite and pyrochlore-based microwave dielectrics.

## 1. Introduction

The perovskite ($ABO_3$) structure is well known to exhibit excellent electrical properties that make it suitable for a variety of electronic applications. Most importantly, the electrical properties can be engineered via chemical modifications in order to obtain insulating, semiconducting, and conducting characteristics.[1-5] In the perovskite structure, the tolerance factor ($t$) is often used to determine the structural stability, which can be calculated from Eq. (1).

$$t = \frac{R_A + R_O}{\sqrt{2}(R_B + R_O)} \qquad (1)$$

where $R_A$, $R_B$, and $R_O$ are the ionic radii of A-cation, B-cation, and oxygen ion, respectively. For ideal cubic perovskites such as $SrTiO_3$ the tolerance factor equals to 1.00. Stable perovskites with non-cubic symmetry can be obtained when the tolerance factor deviates from 1.00. For example, $BaTiO_3$ with a tolerance factor of 1.06 exhibits tetragonal symmetry and $CaTiO_3$ with a tolerance factor of 0.97 exhibits orthorhombic symmetry. However, the perovskite structure is no longer stable when

the tolerance factor greatly deviates from the ideal value ($t$ = 1.00) such as for $MgTiO_3$ ($t$ = 0.81), which is stabilized in the ilmenite structure.

The tolerance factor can also be applied to complex perovskites in which more than one cation occupies the A and/or B sites $(A´A´´)(B´B´´)O_3$. Complex perovskites exhibit structural changes as predicted from the tolerance factor but additional improvement in the electrical properties can be observed.[6-8] For example, the substitution of Zr onto the Ti-site of $PbTiO_3$ results in excellent piezoelectric properties in the widely used material $Pb(Zr_{0.52}Ti_{0.48})O_3$ (PZT).[9] Substitution of Sr onto the Ba-site in $BaTiO_3$ results in a tunable dielectric capacitor $(Ba,Sr)TiO_3$ (BST).[10] Lead-free piezoelectric ceramics with large piezoelectric coefficients can also be obtained in complex perovskites such as the $Ba(Ti_{0.8}Zr_{0.2})O_3$ – $(Ba_{0.7}Ca_{0.3})TiO_3$ system.[11]

Recent research has been focused on the development of high permittivity dielectrics with temperature-stable performance characteristics for capacitor applications requiring high temperatures (> 200 °C). Complex perovskites based on $BaTiO_3$ – $Bi(Me)O_3$ solid solutions have been found to be suitable candidates with promising electrical properties for compounds where the *Me* cation possesses an average charge of 3+. An increase in the mole content of $Bi(Me)O_3$ (with compounds such as $Bi(Zn_{1/2}Ti_{1/2})O_3$, $Bi(Mg_{1/2}Ti_{1/2})O_3$, $Bi(Ni_{1/2}Ti_{1/2})O_3$, $BiScO_3$) leads to an increase in the temperature stability of the permittivity at high temperatures.[12-15] In particular, the $BaTiO_3$ – $Bi(Zn_{1/2}Ti_{1/2})O_3$ – $BiScO_3$ solid solution exhibits a

temperature-stable high permittivity with $\varepsilon_r$ greater than 1000 over the temperature range 100 – 400 °C.[16,17] This family of compounds ($BaTiO_3$ – Bi(*Me*)$O_3$) exhibits weak relaxor ferroelectric behavior which governs the low-field and high-field dielectric behavior.[15] The low-field (i.e. E < 10 kV/cm) dielectric response is characterized by a broad and diffuse temperature dependence of the permittivity. The high-field (i.e. E > 10 kV/cm) dielectric behavior shows a pseudo-linear dielectric response with a high permittivity and negligible saturation.

For capacitor applications, it is desirable to use dielectrics with temperature-stable permittivity characteristics, therefore the capacitor can be operated over a wide temperature range. The temperature coefficient of permittivity ($TC\varepsilon$) is a useful characteristic for determining the temperature stability of dielectric materials and can be obtained from Eq. (2).

$$TC\varepsilon = \frac{1}{\varepsilon}\left(\frac{\partial \varepsilon}{\partial T}\right) \qquad (2)$$

In this work, the tolerance factor of the $BaTiO_3$ – Bi(*Me*)$O_3$ system will be discussed and the low-field dielectric properties will be analyzed in term of the temperature stability as defined by the temperature coefficient of permittivity ($TC\varepsilon$). The important relationship between the tolerance factor and $TC\varepsilon$ will be discussed based on data obtained from the $BaTiO_3$ – Bi(*Me*)$O_3$ compounds as well as relevant phenomenological theories.

## 2. Experimental procedure

Solid solutions based on $BaTiO_3$ – $Bi(Me)O_3$ are the focus of this study, including the solid solutions $BaTiO_3$ – $Bi(Zn_{1/2}Ti_{1/2})O_3$ (BT-BZT), $BaTiO_3$ – $Bi(Zn_{1/2}Ti_{1/2})O_3$ – $BiInO_3$ (BT-BZT-BI), $BaTiO_3$ – $Bi(Zn_{1/2}Ti_{1/2})O_3$ – $BiScO_3$ (BT-BZT-BS), and $BaTiO_3$ – $Bi(Zn_{1/2}Ti_{1/2})O_3$ – $BiScO_3$ – $NaNbO_3$ (BT-BZT-BS-NN). The specific compositions selected for this study are listed in **Error! Reference source not found.** All samples were prepared by using the solid state reaction technique.[17] The dielectric data from previous studies were utilized for further analysis, including measurements at various frequencies from room temperature up to 500 °C.[17-19] The dielectric properties of these solid solutions exhibited a broad and diffuse dielectric peak and it was shown previously that minor modification by the introduction of Ba vacancies could improve the dielectric properties and insulation resistance of the materials.[18] Thus, all compounds selected in this study were nominally A-site non-stoichiometric with a batch composition fixed at 0.02 mol Ba-deficient. The presence of A-site vacancies in the complex perovskite structure will be taken into account in the tolerance factor calculation. The ionic radii required for the calculations were obtained from the data of Shannon and Prewitt.[20] To determine the temperature coefficient of permittivity ($TC\varepsilon$), the permittivity data was selected over an appropriate temperature range for analysis. In this study, the common temperature range that exhibited a monotonic trend in permittivity for all compositions was above the temperature at which the permittivity was maximum ($T_{max}$), which was over the

range of 100 to 400 °C. However, to avoid anomalous permittivity variations near $T_{max}$ and at high temperatures due to conduction losses, the permittivity measured at 1 kHz over temperature range 200 to 400 °C was chosen for calculating the temperature coefficient of permittivity ($TC\varepsilon$).

## 3. Results and discussion

The tolerance factor of selected complex perovskite $BaTiO_3$ – Bi(*Me*)$O_3$ compounds is shown in Table 1. Due to the relatively small cation size of $Bi^{3+}$ (1.36 Å), it can be seen that Bi(*Me*)$O_3$ end-members have low values of the tolerance factor. For example, the tolerance factor values of $Bi(Zn_{1/2}Ti_{1/2})O_3$, $BiInO_3$ and $BiScO_3$ are equal to 0.9417, 0.8871, and 0.9098, respectively, as compared to that of the $BaTiO_3$ end-member ($t$ = 1.0615). Thus, with a decreasing mole fraction of $BaTiO_3$ or increasing mole fraction of Bi(*Me*)$O_3$, the result is a decrease in the tolerance factor of the solid solution. In terms of ion size, the increase in concentration of larger B-cations ($Zn^{2+}$, $In^{3+}$, and $Sc^{3+}$) and the decrease in concentration of larger A-cation ($Ba^{2+}$) result in a lowering of the tolerance factor in $BaTiO_3$ – Bi(*Me*)$O_3$. It is noted that the ionic radii of $Ba^{2+}$ and $Bi^{3+}$ occupying the 12-fold coordinated site are 1.61 and 1.36 Å, respectively, and the ionic radii of $Ti^{4+}$, $Zn^{2+}$, $In^{3+}$, and $Sc^{3+}$ occupying 6-fold coordinated site are 0.605, 0.740, 0.800, and 0.745 Å, respectively.[20,21]

Table 1 Compositions and calculated tolerance factor (*t*) of

$BaTiO_3 – Bi(Me)O_3$ solid solutions

| Composition | *t* |
|---|---|
| $0.80BaTiO_3 – 0.20Bi(Zn_{1/2}Ti_{1/2})O_3$ | 1.0256 |
| $0.80BaTiO_3 – 0.10Bi(Zn_{1/2}Ti_{1/2})O_3 – 0.10BiInO_3$ | 1.0192 |
| $0.75BaTiO_3 – 0.125Bi(Zn_{1/2}Ti_{1/2})O_3 – 0.125BiInO_3$ | 1.0116 |
| $0.60BaTiO_3 – 0.20Bi(Zn_{1/2}Ti_{1/2})O_3 – 0.20BiScO_3$ | 0.9943 |
| $0.55BaTiO_3 – 0.225Bi(Zn_{1/2}Ti_{1/2})O_3 – 0.225BiScO_3$ | 0.9875 |
| $0.50BaTiO_3 – 0.25Bi(Zn_{1/2}Ti_{1/2})O_3 – 0.25BiScO_3$ | 0.9807 |
| $0.70BaTiO_3 – 0.10Bi(Zn_{1/2}Ti_{1/2})O_3 – 0.10BiScO_3 – 0.10NaNbO_3$ | 1.0249 |
| $0.60BaTiO_3 – 0.15Bi(Zn_{1/2}Ti_{1/2})O_3 – 0.15BiScO_3 – 0.10NaNbO_3$ | 1.0114 |
| $0.50BaTiO_3 – 0.10Bi(Zn_{1/2}Ti_{1/2})O_3 – 0.10BiScO_3 – 0.30NaNbO_3$ | 1.0060 |
| $0.50BaTiO_3 – 0.15Bi(Zn_{1/2}Ti_{1/2})O_3 – 0.15BiScO_3 – 0.20NaNbO_3$ | 1.0019 |
| $0.45BaTiO_3 – 0.175Bi(Zn_{1/2}Ti_{1/2})O_3 – 0.175BiScO_3 – 0.20NaNbO_3$ | 0.9951 |
| $0.40BaTiO_3 – 0.20Bi(Zn_{1/2}Ti_{1/2})O_3 – 0.20BiScO_3 – 0.20NaNbO_3$ | 0.9883 |

The tolerance factor of $BaTiO_3 – Bi(Zn_{1/2}Ti_{1/2})O_3$, $BaTiO_3 – Bi(Zn_{1/2}Ti_{1/2})O_3 – BiInO_3$, $BaTiO_3 – Bi(Zn_{1/2}Ti_{1/2})O_3 – BiScO_3$, and $BaTiO_3 – Bi(Zn_{1/2}Ti_{1/2})O_3 – BiScO_3 – NaNbO_3$ compounds were varied from greater than 1 to lower than 1, which suggests a non-cubic crystal structure. However, structural characterization by X-ray

diffraction showed that the compounds exhibited a pseudocubic crystal structure, which could also be found in other related systems with similar tolerance factors, for example, $BaTiO_3$ – $BiScO_3$,[15] $BaTiO_3$ – $Bi(Mg_{1/2}Ti_{1/2})O_3$,[13] and $BaTiO_3$ – $Bi(Ni_{1/2}Ti_{1/2})O_3$.[14] In-depth structural characterizations of $BaTiO_3$ – $Bi(Zn_{1/2}Ti_{1/2})O_3$ by using high resolution synchrotron X-ray diffraction (HRXRD) and neutron pair distribution function (NPDF) techniques indicated that long-range structure of the compounds are indeed pseudocubic, however the local structure (nanoscale) was found to be non-cubic. This is likely a common occurrence in $BaTiO_3$ – $Bi(Me)O_3$ solid solutions. It can be seen that the structure suggested from tolerance factor considerations and the structure observed by using high resolution diffraction techniques were in a good agreement in considering short-range structure.

The temperature coefficient of permittivity ($TC\varepsilon$) of compounds listed in Table 1 were found to be in the range of -2441 to -182 ppm/°C.[17] As the concentration of the $Bi(Me)O_3$ component increased, the $|TC\varepsilon|$ decreased reaching values close to zero indicating that compositions with high concentrations of $Bi(Me)O_3$ exhibited stable dielectric properties. In this case, the composition with the optimum $TC\varepsilon$ was $0.50BaTiO_3 – 0.25Bi(Zn_{1/2}Ti_{1/2})O_3 – 0.25BiScO_3$ with a value of $TC\varepsilon$ = -182 ppm/°C. It should be noted that this composition was near the solubility limit of this solid solution. Similar behavior was observed in the $BaTiO_3$ – $Bi(Me)O_3$ system with different $Bi(Me)O_3$ end-members,[12-16] however, $TC\varepsilon$ values were not reported for these systems. The variation of $TC\varepsilon$ as a function of tolerance factor of selected

$BaTiO_3$ – Bi(*Me*)$O_3$ compositions is shown in Fig. 1. A monotonic trend could be observed in which the $TC\varepsilon$ values (-2441 to -182 ppm/°C) approach zero as the tolerance factor decreased from 1.0256 to 0.9807. The pseudo-quaternary compounds of BT-BZT-BS-$NaNbO_3$ showed the same trend with the tolerance factor and the $TC\varepsilon$, as shown in Fig. 1.

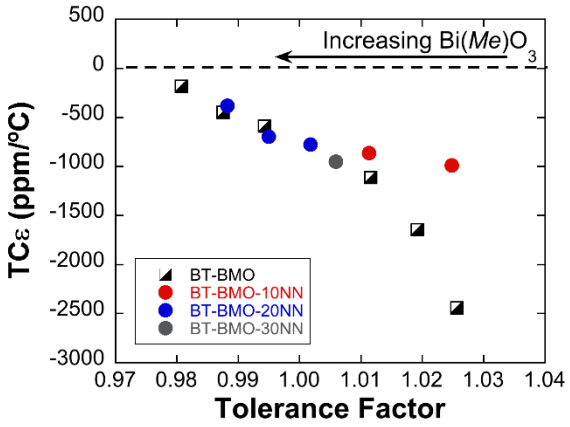


Fig. 1. Temperature coefficient of permittivity ($TC\varepsilon$) versus tolerance factor of selected $BaTiO_3$ – Bi(*Me*)$O_3$ compounds

A dispersion of $TC\varepsilon$ values could be observed for compositions exhibiting tolerance factor greater than 1.01. By comparing the 0.8BT-0.2BZT ($t$ = 1.0256) and the 0.7BT-0.1BZT-0.1BS-0.1NN ($t$ = 1.0249) compositions, the differences in the $TC\varepsilon$ values could be due to the interruption of long range order of polar regions by multi-cations occupying B-site of the latter compound as compare to the former

compound. However, the BT-BZT-BS-NN system produces dielectrics with overall lower relative permittivities compared to the other compositions presented in this investigation. Compositions with more $BaTiO_3$ exhibited higher dielectric constants and tolerance factors but also higher temperature dependence of permittivity.

Based on the trend observed in Fig.1, it is clear that further reduction of tolerance factor could potentially lead to an improvement in $TC\varepsilon$ to obtain temperature-stable high permittivity dielectrics ($TC\varepsilon \approx 0$). However, further increasing the Bi($Me$)$O_3$ concentration from the $0.50BaTiO_3 - 0.25Bi(Zn_{1/2}Ti_{1/2})O_3 - 0.25BiScO_3$ composition is not possible as it would exceed the solubility limit of the system, leading to the formation of secondary phases and a consequent degradation in electrical properties. Therefore, to avoid the formation of secondary phases in the system, A-cation (Ba or Bi) substitutions with an isovalent cation was considered. Specifically, the cations Sr and Ca were selected as dopant elements to substitute for the Ba ion in the $0.50BaTiO_3 - 0.25Bi(Zn_{1/2}Ti_{1/2})O_3 - 0.25BiScO_3$ compositions. This resulted in lowering the tolerance factor from 0.9807 (undoped) to 0.9749 (Sr-doped) and 0.9714 (Ca-doped). Secondary phases were not detected by x-ray diffraction within the resolution limit of the laboratory scale instrument. Since the ionic radii of $Sr^{2+}$ (1.44 Å) and $Ca^{2+}$ (1.34 Å) were smaller than that of $Ba^{2+}$ (1.61 Å), thus, it led to the reduction in the average $R_A - R_O$ distance resulting in a decrease in tolerance factor for the Sr and Ca-substituted compounds.

The temperature dependence of the relative permittivity of Sr-doped and Ca-doped $0.50BaTiO_3 - 0.25Bi(Zn_{1/2}Ti_{1/2})O_3 - 0.25BiScO_3$ compounds is shown in Fig 2. Temperature stable behavior was maintained for both materials as the $TC\varepsilon$ values of Sr-doped and Ca-doped compositions approached zero as compared to that of the undoped composition. The substitution of Sr had only a moderate effect on improving the temperature stability, however, the $TC\varepsilon$ values transitioned from -100 ppm/°C to +100 ppm/ºC in the Ca-doped compositions. For both cases, the permittivity decreased as the doping concentration increased. The permittivity of all Sr-doped compounds remained higher than 1000. However, permittivities values of less than 1000 were obtained in the Ca-doped compounds. These results suggest that Ca is an effective dopant in the $0.50BaTiO_3 - 0.25Bi(Zn_{1/2}Ti_{1/2})O_3 - 0.25BiScO_3$ system for achieving temperature stable dielectric properties.

These results show that decreasing the tolerance factor via the substitution of Sr and Ca ions for Ba successfully shifted the $TC\varepsilon$ closer to zero. A different rate of the change in the value of $TC\varepsilon$ and the unit cell volume was observed for Sr-doped and Ca-doped compositions as shown in Fig.3. Comparatively, at approximately the same tolerance factor for Sr-doped and Ca-doped compositions, the difference in $TC\varepsilon$ value was significant (~60 ppm/°C). Following the model proposed by Levin, see Ref. 21, this difference can be explained by the different bonding nature of the substituting ions (Sr and Ca).[22] In the case of Sr substitution for Ba in $BaTiO_3$, a reduction in unit cell volume is observed as well as a more relaxed bonding nature for Sr-O in $[SrO_{12}]$

coordination. The substitution of the Ca ion for Ba in $BaTiO_3$ resulted in a reduced unit cell volume and an off-center position for Ca, resulting in a strained Ca-O bond, in $[CaO_{12}]$ coordination, similar to the results obtained by Zheng.[23]

This strained Ca-O bond can induce stress in the lattice, which could interrupt or clamp the polarization dynamics resulting in a reduction in permittivity and a stabilization of the permittivity over a wide temperature range.[24] Based on this analysis, it is suggested that the unit cell volume reduction and the strained Ca-O bonding characteristic played a major role in the significant reduction of permittivity. This could also mean that the presence of the strained Ca-O bond helped further stabilize the permittivity as the temperature increased. This result supports the correlated rattling-ion model recently proposed by Krayzman *et al.* with the $BaTiO_3$ – $BiScO_3$ solid solution. This model would suggest that the substitution of Sr or Ca for Ba impacts the Bi off-centering and split-site separation therefore resulting in a modification of the dielectric behavior.[25]

The temperature dependence of the relative permittivity of $BaTiO_3$ – $Bi(Zn_{1/2}Ti_{1/2})O_3$ – $BiScO_3$ – $NaNbO_3$ compounds is shown in Fig. 4. The addition of $NaNbO_3$ was effective in shifting the temperature of the dielectric maximum ($T_{max}$) to temperatures as low as -50°C. While this shift resulted in lower room temperature dielectric loss values it was also accompanied with a lower permittivity. These results show that decreasing the tolerance factor in this system lowers the temperature coefficient of permittivity. Dielectric constant, dielectric loss at room temperature

and temperature coefficient of permittivity determined from 30 – 200 °C are shown in Table 2.

The temperature coefficient of permittivity and tolerance factor relationship has been studied in detail for (Ba/Sr)($Me_{1/3}$(Nb/Ta)$_{2/3}$)$O_3$ microwave dielectrics ($\varepsilon_r \approx 40$) with similar results to the present work.[26] Reaney *et al.* showed that as the tolerance factor decreased ($t < 0.9900$), the $TC\varepsilon$ values transitioned from negative to positive values. Additionally, it was found that the microwave dielectric compounds with tolerance factors in the range of 0.9850 to 0.9650 exhibited the $TC\varepsilon$ values close to zero, which corresponded to structures with anti-phase octahedral tilting. Compared to this study, as shown in Fig. 3(a), the compounds with $t < 0.9900$ exhibited the $TC\varepsilon$ values close to zero with a negative to positive transition. This finding suggests that both groups of materials share a common relationship between the temperature coefficient of permittivity and the tolerance factor.

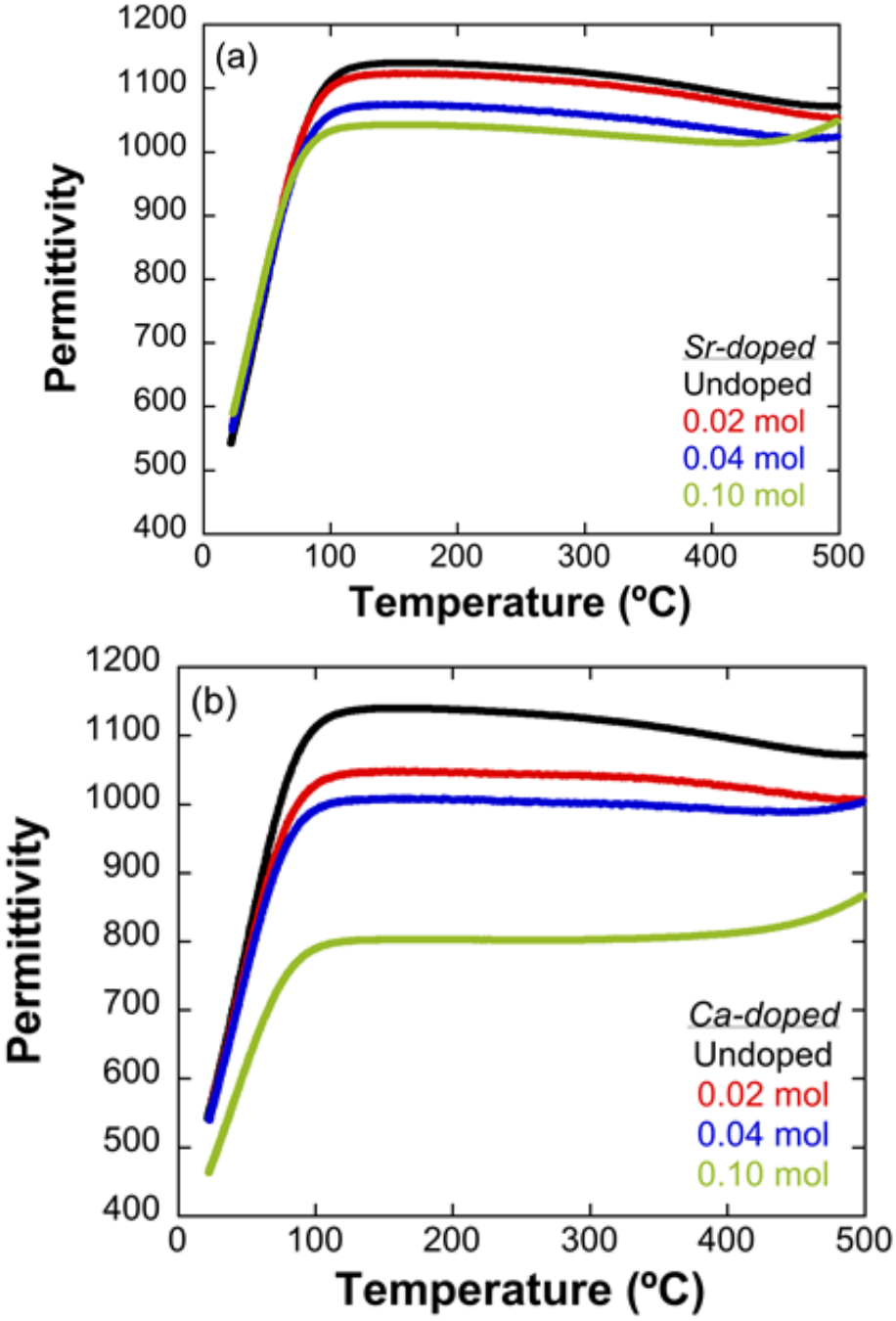


Fig. 15. Temperature dependence of permittivity of (a) Sr-doped and (b) Ca-doped $0.50BaTiO_3 – 0.25Bi(Zn_{1/2}Ti_{1/2})O_3 – 0.25BiScO_3$ compounds

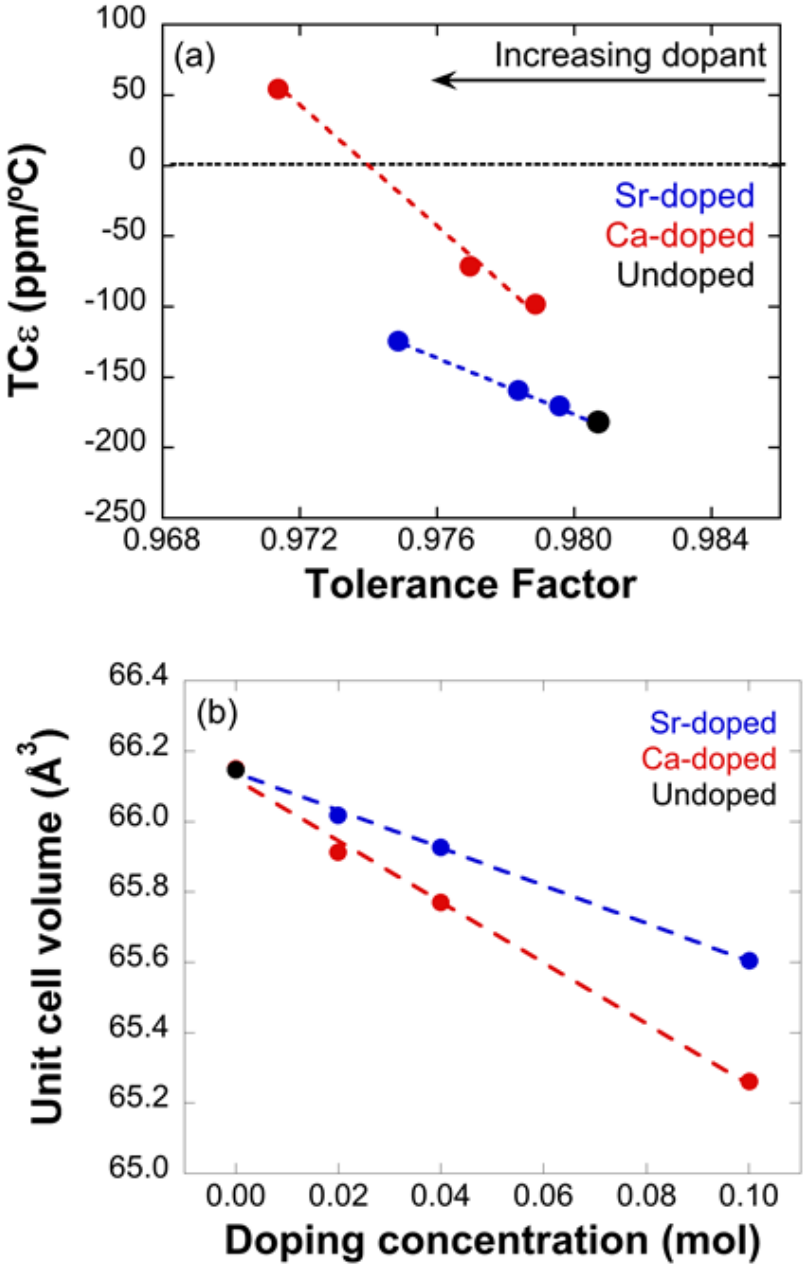


Fig. 3. (a) Temperature coefficient of permittivity ($TC\varepsilon$) versus tolerance factor and (b) unit cell volume as a function of doping concentration for Sr-doped and Ca-doped $0.50BaTiO_3 – 0.25Bi(Zn_{1/2}Ti_{1/2})O_3 – 0.25BiScO_3$ compounds

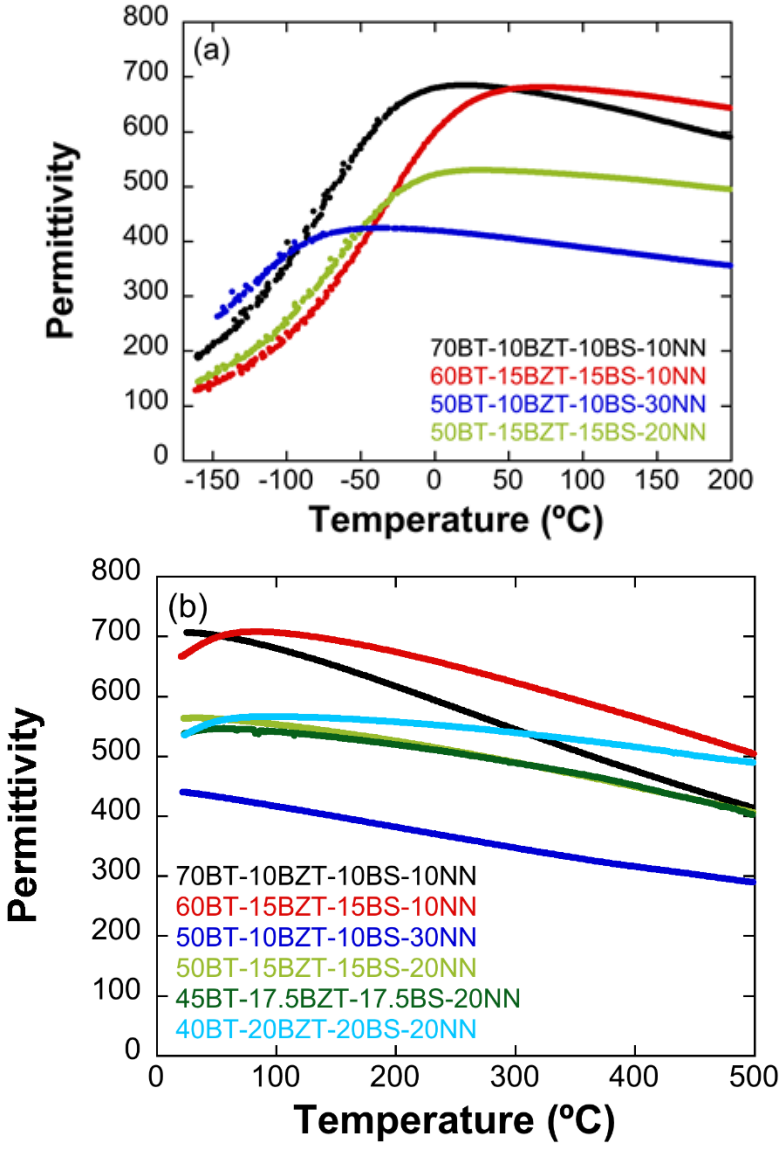
(a)
Permittivity
Temperature (ºC)
70BT-10BZT-10BS-10NN
60BT-15BZT-15BS-10NN
50BT-10BZT-10BS-30NN
50BT-15BZT-15BS-20NN
(b)
Permittivity
Temperature (ºC)
70BT-10BZT-10BS-10NN
60BT-15BZT-15BS-10NN
50BT-10BZT-10BS-30NN
50BT-15BZT-15BS-20NN
45BT-17.5BZT-17.5BS-20NN
40BT-20BZT-20BS-20NN

Fig. 4 Temperature dependence of permittivity of $BaTiO_3 – Bi(Zn_{1/2}Ti_{1/2})O_3 – BiScO_3 – NaNbO_3$ compounds at (a) low temperatures and (b) high temperatures

Table 2. $BaTiO_3 – Bi(Zn_{1/2}Ti_{1/2})O_3 – BiScO_3 – NaNbO_3$ compounds with permittivity and dielectric loss (tan δ) at room temperature and temperature coefficient of permittivity ($TC\varepsilon$)

| Compounds | Permittivity (room temperature) | tan δ (room temperature) | $TC\epsilon$ (ppm/°C) (30 – 200 °C) |
|---|---|---|---|
| 70BT-10BZT-10BS-10NN | 706 | 0.011 | -789 |
| 60BT-15BZT-15BS-10NN | 670 | 0.052 | -476 |
| 50BT-10BZT-10BS-30NN | 439 | 0.003 | -818 |
| 50BT-15BZT-15BS-20NN | 563 | 0.014 | -412 |
| 45BT-17.5BZT-17.5BS-20NN | 537 | 0.028 | -231 |
| 40BT-20BZT-20BS-20NN | 536 | 0.048 | 159 |

The temperature dependence of the permittivity of $(Ba/Sr)(Me_{1/3}(Nb/Ta)_{2/3})O_3$ microwave dielectrics and other cubic compounds was explained by Colla *et al.*,[27] Bosman and Havinga,[28] Cockbain and Harrop,[29] and Harrop.[30] The analysis of the macroscopic Clausius-Mossotti formula with respect to temperature showed that three physical processes contribute to the temperature dependence of permittivity in cubic compounds. First, there is an increase in macroscopic polarizability due to volume expansion. Second, there is a decrease in the number of polarizable particles per unit

volume as the temperature increases because of the effect of volume expansion. Third, at constant volume, there is an intrinsic temperature dependence of the macroscopic polarizability. Based on these mechanisms, the macroscopic polarizability plays a major role in controlling the temperature dependence of the permittivity. However, due to the complicated contribution of the polarizability from multiple mechanisms in complex perovskites,[28,29] a revised analysis of the Clausius-

Mossotti relationship is needed in order to successfully explain the temperature dependence of permittivity of high permittivity complex perovskites such as the dielectric materials in this work.

Pyrochlore-based dielectrics are known to exhibit temperature-stable permittivity characteristics, similar to perovskite, with permittivities of approximately 200 or less. Researchers have focused on the development of Bi-based pyrochlores due to their excellent electrical properties for microwave dielectric applications.[31-37] The temperature coefficient of permittivity ($TC\varepsilon$) of Bi-based pyrochlores was found to be in the range of -1330 ppm/ºC to values close to zero. Valant and Davies showed that the $TC\varepsilon$ values approached zero as the ratio of A-cation and B-cation radii ($R_A/R_B$) decreased in a manner such that $R_A/R_B$ was used to represent the stability of pyrochlore.[37] Due to difference in structural characteristics between pyrochlore and perovskite, the tolerance factor used for perovskite cannot be directly applied to pyrochlore. Recenlty, Cai *et al.* re-defined the tolerance factor of pyrochlore by considering the two distinct tetrahedra ($A_2B_2$ and $A_4$ with oxygen inside) that comprise the pyrochlore structure.[38] Two tolerance factors were determined by Eqs. (3) and (4), as follows;

$$t_1 = \frac{\sqrt{\left(x-\frac{1}{4}\right)^2+\frac{1}{32}}}{\sqrt{\left(x-\frac{1}{2}\right)^2+\frac{1}{32}}}\left(\frac{R_A+R_O}{R_B+R_O}\right) \qquad (3)$$

$$t_2 = a\left(\frac{3\sqrt{3}}{8(R_A+R_O)}\right) \qquad (4)$$

where, $t_1$ represents tolerance factor of the $A_2B_2$ tetrahedra with O inside, x represents the Wyckoff position of oxygen at 48f (x, 1/8, 1/8), $t_2$ represents the tolerance factor of the $A_4$ tetrahedra with O´ inside, and $a$ represents the lattice parameter of the pyrochlore unit cell. Previous works by Kamba *et al.*[33] and Nino[39] suggested that dominant dielectric response of Bi-based pyrochlores originates from O´-A-O´ bonding dynamics. Therefore, it is suggested to consider $t_2$ as the parameter to correlate with the dielectric response of pyrochlore structures since it is closely related to A-O´ bonding. The linear relationship between $t_2$ and $R_A/R_B$ was determined in which $t_2$ decreased linearly as $R_A/R_B$ increased.[38] It should be noted that the majority of pyrochlore compounds possess $t_2$ values in between 0.8800 to 0.9200. However, the relationship between the $TC\varepsilon$ and the $t_2$ was not presented. Thus, in order to investigate this relationship, the $t_2$ and the $TC\varepsilon$ of (Bi,Zn)(Ti,Nb)$O_7$ pyrochlores were extracted from Cai *et al.*[38] and Valant and Davies,[36] respectively, and is shown in Table 2. It could be seen that as the $t_2$ increased the $TC\varepsilon$ values approached zero. Since $t_2$ showed a linear relationship with $R_A/R_B$ as previously mentioned, for pyrochlores the $TC\varepsilon$ approached zero when $t_2$ increased or $R_A/R_B$ decreased.

Table 2 Bi-based pyrochlore compounds and associated tolerance factor ($t_2$), and temperature coefficient of permittivity ($TC\varepsilon$)

| Compounds | $t_2$[38] | $TC\epsilon$ (ppm/ºC)[36] |
|---|---|---|
| $(Bi_{1.65}Zn_{0.35})(Ti_{1.65}Nb_{0.35})O_7$ | 0.8970 | -1330 |
| $(Bi_{1.50}Zn_{0.50})(Ti_{1.50}Nb_{0.50})O_7$ | 0.9030 | -1300 |
| $(Bi_{1.00}Zn_{1.00})(Ti_{1.00}Nb_{1.00})O_7$ | 0.9260 | -870 |

In general, the relationship between the tolerance factor and the temperature coefficient of permittivity ($TC\varepsilon$) was established for temperature-stable high permittivity $BaTiO_3$ – Bi($Me$)$O_3$ compounds, i.e., as the tolerance factor decreased, the $TC\varepsilon$ approached zero. This relationship was found to be similar to that of microwave dielectric Ba- and Sr-based perovskites. In comparison with Bi-based pyrochlore compounds, the $TC\varepsilon$ approached zero when the tolerance factor ($t_2$), defined differently as compared to perovskites, increased or $R_A/R_B$ decreased. Overall, the established structure-property relationships for high permittivity perovskites, microwave dielectric perovskites, and microwave dielectric pyrochlores can be a useful guide for developing new high-permittivity materials with temperature-stable behavior.

## 4. Conclusions

As the tolerance factor decreased from 1.0256 to 0.9807 due to the addition of Bi($Me$)$O_3$ in $BaTiO_3$ – Bi($Me$)$O_3$ compounds, the result was a shift in the temperature dependence of permittivity ($TC\varepsilon$) to values approaching zero (from -2441 to -182 ppm/ºC). This suggests that the $TC\varepsilon$ can be optimized by engineering the tolerance factor by designing the composition of perovskite solid solutions. The substitution of Ba in the $0.50BaTiO_3 – 0.25Bi(Zn_{1/2}Ti_{1/2})O_3 – 0.25BiScO_3$ solid solution with Sr or Ca resulted in a decrease in tolerance factor, a decrease in the unit cell volume, and a decreased permittivity. However, the temperature stability of the permittivity for Sr-doped and Ca-doped was significantly improved. The bonding nature of Sr-O (relaxed) and Ca-O (strained) played a significant role in governing the magnitude of the permittivity and the $TC\varepsilon$. The range of tolerance factors that shifted $TC\varepsilon$ values close to zero was found to be similar to that observed in high permittivity perovskite-based microwave dielectrics ($t \approx 0.9750$-$0.9800$). This study suggests a general relationship between $TC\varepsilon$ and the tolerance factor, which can be used as a guide to design new high permittivity compounds with temperature-stable permittivity characteristics.

**References**

[1]S. Jin, T. H. Tiefel, M. Mccormack, R. A. Fastnacht, R. Ramesh, and L. H. Chen, Thousandfold change in resistivity in magnetoresistive La-Ca-Mn-O films, *Science*, **264**, 413 (1994).

[2]N. Q. Minh, Ceramic Fuel-Cells, *J. Am. Ceram. Soc.*, **76**, 563 (1993).

[3]Y. Saito, H. Takao, T. Tani, T. Nonoyama, K. Takatori, T. Homma, T. Nagaya, and M. Nakamura, Lead-free piezoceramics, *Nature*, **432**, 84 (2004).

[4]R. Waser, R. Dittmann, G. Staikov, and K. Szot, Redox-based resistive switching memories - nanoionic mechanisms, prospects, and challenges, *Adv. Mater.*, **21**, 2632 (2009).

[5]K. D. Kreuer, Proton conductivity: materials and applications, *Chem. Mater.*, **8**, 610 (1996).

[6]A. A. Bokov and Z. G. Ye, Recent progress in relaxor ferroelectrics with perovskite structure, *J. Mater. Sci*., **41**, 31 (2006).

[7]B. Noheda, D. E. Cox, G. Shirane, J. Gao, and Z. G. Ye, Phase diagram of the ferroelectric relaxor (1-x)$PbMg_{1/3}Nb_{2/3}O_3$-(x)$PbTiO_3$, *Phys. Rev. B.*, **66**, 054104 (2002).

[8]C. S. Tu, I. G. Siny, and V. H. Schmidt, Sequence of Dielectric anomalies and high-temperature relaxation behavior in $Na_{1/2}Bi_{1/2}TiO_3$, *Phys. Rev. B.*, **49**, 11550 (1994).

[9]R. Guo, L. E. Cross, S. E. Park, B. Noheda, D. E. Cox, and G. Shirane, Origin of the high piezoelectric response in $PbZr_{1-x}Ti_xO_3$, *Phys. Rev. Lett.*, **84**, 5423 (2000).

[10]A. K. Tagantsev, V. O. Sherman, K. F. Astafiev, J. Venkatesh, and N. Setter, Ferroelectric materials for microwave tunable applications, *J. Electroceram*., **11**, 5 (2003).

[11]W. F. Liu and X. B. Ren, Large Piezoelectric effect in Pb-free ceramics, *Phys. Rev. Lett.*, **103**, 257602 (2009).

[12]C. C. Huang and D. P. Cann, Phase transitions and dielectric properties in $Bi(Zn_{1/2}Ti_{1/2})O_3$-$BaTiO_3$ perovskite solid solutions, *J. Appl. Phys.*, **104**, 024117 (2008).

[13]B. Xiong, H. Hao, S. J. Zhang, H. X. Liu, and M. H. Cao, Structure, dielectric properties and temperature stability of $BaTiO_3$-$Bi(Mg_{1/2}Ti_{1/2})O_3$ perovskite solid solutions, *J. Am. Ceram. Soc.*, **94**, 3412 (2011).

[14]I. Fujii, K. Nakashima, N. Kumada, and S. Wada, Structural, dielectric, and piezoelectric properties of $BaTiO_3$-$Bi(Ni_{1/2}Ti_{1/2})O_3$ ceramics, *J. Ceram. Soc. Jpn*., **120**, 30 (2012).

[15]H. Ogihara, C. A. Randall, and S. Trolier-McKinstry, Weakly coupled relaxor behavior of $BaTiO_3$-$BiScO_3$ ceramics, *J. Am. Ceram. Soc.*, **92**, 110 (2009).

[16]C. C. Huang, D. P. Cann, X. Tan, and N. Vittayakorn, Phase transitions and ferroelectric properties in $BiScO_3$-$Bi(Zn_{1/2}Ti_{1/2})O_3$-$BaTiO_3$ solid solutions, *J. Appl. Phys.*, **102**, 044103 (2007).

[17]N. Raengthon, T. Sebastian, D. Cumming, I. M. Reaney, and D. P. Cann, $BaTiO_3$-$Bi(Zn_{1/2}Ti_{1/2})O_3$-$BiScO_3$ ceramics for high-temperature capacitor applications, *J. Am. Ceram. Soc.*, **95**, 3554 (2012).

[18]N. Raengthon and D. P. Cann, Dielectric relaxation in $BaTiO_3$-$Bi(Zn_{1/2}Ti_{1/2})O_3$ ceramics, *J. Am. Ceram. Soc.*, **95**, 1604 (2012).

[19]N. Raengthon and D. P. Cann, High temperature electronic properties of $BaTiO_3$-$Bi(Zn_{1/2}Ti_{1/2})O_3$-$BiInO_3$ for capacitor applications, *J. Electroceram.*, **28**, 165 (2012).

[20]R. D. Shannon and C. T. Prewitt, Effective ionic radii in oxides and fluorides, *Acta. Crystallogr.*, **B25**, 925 (1969).

[21]M. R. Suchomel and P. K. Davies, Predicting the position of the morphotropic phase boundary in high temperature $PbTiO_3$-$Bi(B'B'')O_3$ based dielectric ceramics, *J. Appl. Phys.*, **96**, 4405 (2004).

[22]I. Levin, V. Krayzman, and J. C. Woicik, Local-structure origins of the sustained Curie temperature in $(Ba,Ca)TiO_3$ ferroelectrics, *Appl. Phys. Lett.*, **102**, 162906 (2013).

[23]R. K. Zheng, J. Wang, X. G. Tang, Y. Wang, H. L. W. Chan, C. L. Choy, and X. G. Li, Effects of Ca doping on the Curie temperature, structural, dielectric, and elastic properties of $Ba_{0.4}Sr_{0.6-x}Ca_xTiO_3$ ($0 <= x <= 0.3$) perovskites, *J. Appl. Phys.*, **98**, 084108 (2005).

[24]G. A. Samara, The relaxational properties of compositionally disordered $ABO_3$ perovskites, *J. Phys. Condens. Matter.*, **15**, R367 (2003).

[25]V. Krayzman, I. Levin, J. C. Woicik, and F. Bridges, Correlated rattling-ion origins of dielectric properties in reentrant dipole glasses $BaTiO_3$ – $BiScO_3$, *Appl. Phys. Lett.*, **107**, 192903 (2015).

[26]I. M. Reaney, E. L. Colla, and N. Setter, Dielectric and structural characteristics of Ba-based and Sr-based complex perovskites as a function of tolerance factor, *Jpn. J. Appl. Phys.*, **33**, 3984 (1994).

[27]E. L. Colla, I. M. Reaney, and N. Setter, Effect of structural-changes in complex perovskites on the temperature-coefficient of the relative permittivity, *J. Appl. Phys.*, **74**, 3414 (1993).

[28]A. J. Bosman and E. E. Havinga, Temperature dependence of dielectric constants of cubic ionic compounds, *Phys. Rev.*, **129**, 1593 (1963).

[29]A. G. Cockbain and P. J. Harrop, The temperature coefficient of capacitance, *Brit. J. Appl. Phys.*, **1**, 1109 (1968).

[30]P. J. Harrop, Temperature coefficient of capacitance of solids, *J. Mater. Sci.*, **4**, 370 (1969).

[31]C. Ang, Z. Yu, H. J. Youn, C. A. Randall, A. S. Bhalla, L. E. Cross, and M. Lanagan, Dielectric properties of $Bi_2O_3$-ZnO-$Ta_2O_5$ pyrochlore and zirconolite structure ceramics, *Appl. Phys. Lett.*, **82**, 3734 (2003).

[32]D. P. Cann, C. A. Randall, and T. R. Shrout, Investigation of the dielectric properties of bismuth pyrochlores, *Solid. State. Commun.*, **100**, 529 (1996).

[33]S. Kamba, V. Porokhonskyy, A. Pashkin, V. Bovtun, J. Petzelt, J. C. Nino, S. Trolier-McKinstry, M. T. Lanagan, and C. A. Randall, Anomalous broad dielectric relaxation in $Bi_{1.5}Zn_{1.0}Nb_{1.5}O_7$ pyrochlore, *Phys. Rev. B.*, **66**, 054106 (2002).

[34]C. C. Khaw, K. B. Tan, and C. K. Lee, High temperature dielectric properties of cubic bismuth zinc tantalate, *Ceram. Int*., **35**, 1473 (2009).

[35]J. C. Nino, M. T. Lanagan, and C. A. Randall, Dielectric relaxation in $Bi_2O_3$-ZnO-$Nb_2O_5$ cubic pyrochlore, *J. Appl. Phys*., **89**, 4512 (2001).

[36]M. Valant and P. K. Davies, Synthesis and dielectric properties of pyrochlore solid solutions in the $Bi_2O_3$-ZnO-$Nb_2O_5$-$TiO_2$ system, *J. Mater. Sci.*, **34**, 5437 (1999).

[37]M. Valant and P. K. Davies, Crystal chemistry and dielectric properties of chemically substituted $(Bi_{1.5}Zn_{1.0}Nb_{1.5})O_7$ and $Bi_2(Zn_{2/3}Nb_{4/3})O_7$ pyrochlores, *J. Am. Ceram. Soc.*, **83**, 147 (2000).

[38]L. Cai, A. L. Arias, and J. C. Nino, The tolerance factors of the pyrochlore crystal structure, *J. Mater. Chem*., **21**, 3611 (2011).

[39]J. C. Nino, Fundamental structure-property relationships towards engineering of an integrated NPO capacitor for bismuth pyrochlore systems, Ph.D. Thesis, The Pennsylvania State University, May 2002.

| Compound | Sintering T (ºC) |
|---|---|
| 70BT-10BZT-10BS-10NN | 1200 |
| 60BT-15BZT-15BS-10NN | 1150 |
| 50BT-10BZT-10BS-30NN | 1150 |
| 50BT-15BZT-15BS-20NN | 1150 |
| 45BT-17.5BZT-17.5BS-20NN | 1100 |
| 40BT-20BZT-20BS-20NN | 1100 |

| Compound | $TC\varepsilon_{high}$ (ppm/ºC) | $TC\varepsilon_{mid}$ (ppm/ºC) | $-TC\varepsilon_{low}$ (ppm/ºC) | $T_{max}$ (ºC) | $\varepsilon$ at $T_{max}$ |
|---|---|---|---|---|---|
| 70BT-10BZT-10BS-10NN | -995 | -789 | 708 | 20.5 | 684.18 |
| 60BT-15BZT-15BS-10NN | -870 | -476 | 2,551 | 73.1 | 680.54 |
| 50BT-10BZT-10BS-30NN | -958 | -818 | -549 | -27.5 | 423.39 |
| 50BT-15BZT-15BS-20NN | -783 | -412 | 1,104 | 28.5 | 529.35 |
| 45BT-17.5BZT-17.5BS-20NN | -704 | -231 | - | 56.7 | 545.50 |
| 40BT-20BZT-20BS-20NN | -387 | 159 | - | 95.1 | 565.33 |

| Compound | Sintering T (°C) |
|---|---|
| 55BT-20BZT-25PNN | 1100 |
| 55BT-25BZT-20PNN | 1100 |
| 50BT-30BZT-20PNN | 1100 |
| 50BT-25BZT-25PNN | 1100 |
| 45BT-25BZT-30PNN | 1050 |
| 49BT-29BZT-22PNN | 1050 |

| Compound | $TC\varepsilon_{high}$ (ppm/°C) |
|---|---|
| 55BT-20BZT-25PNN | -1609 |
| 55BT-25BZT-20PNN | -1357 |
| 50BT-30BZT-20PNN | -860 |
| 50BT-25BZT-25PNN | -1289 |
| 45BT-25BZT-30PNN | -1621 |
| 49BT-29BZT-22PNN | -1283 |